Evaluation of IL-1 blockade as an adjunct to linezolid therapy for tuberculosis in mice and macaques

Caylin G. Winchell[1], Bibhuti B. Mishra [2,3], Jia Yao Phuah[2], Mohd Saqib[3], Samantha J. Nelson[2], Pauline Maiello[1], Chelsea M. Causgrove[1], Cassaundra L. Ameel[1], Brianne Stein[1], H. Jacob Borish[1], Alexander G. White[1], Edwin C. Klein[4], Matthew D. Zimmerman[5], Véronique Dartois[5], Philana Ling Lin[6], Christopher M. Sassetti[2], JoAnne L. Flynn[1*]

[1]Department of Microbiology and Molecular Genetics, University of Pittsburgh School of Medicine, Pittsburgh, Pennsylvania, USA

[2]Department of Microbiology and Physiological Systems, University of Massachusetts Medical School, Worcester, Massachusetts, USA

[3]Department of Immunology and Microbial Disease, Albany Medical College, Albany, New York, USA

[4]Division of Laboratory Animal Research, University of Pittsburgh, Pittsburgh Pennsylvania, USA

[5]Center for Discovery and Innovation, Hackensack Meridian Health, Nutley, New Jersey, USA

[6]Department of Pediatrics, UPMC Children's Hospital of the University of Pittsburgh, Pittsburgh, Pennsylvania, USA

* **Corresponding author**
JoAnne L. Flynn
Email: joanne@pitt.edu

Keywords: Tuberculosis, MDR-TB, IL-1, Linezolid, host-directed therapy

Abstract

In 2017 over 550,000 estimated new cases of multi-drug/rifampicin resistant tuberculosis (MDR/RR-TB) occurred, emphasizing a need for new treatment strategies. Linezolid (LZD) is a potent antibiotic for drug-resistant Gram-positive infections and is an effective treatment for TB. However, extended LZD use can lead to LZD-associated host toxicities, most commonly bone marrow suppression. LZD toxicities may be mediated by IL-1, an inflammatory pathway important for early immunity during *M. tuberculosis* infection. However, IL-1 can contribute to pathology and disease severity late in TB progression. Since IL-1 may contribute to LZD toxicity and does influence TB pathology, we targeted this pathway with a potential host-directed therapy (HDT). We hypothesized LZD efficacy could be enhanced by modulation of IL-1 pathway to reduce bone marrow toxicity and TB associated-inflammation. We used two animal models of TB to test our hypothesis, a TB-susceptible mouse model and clinically relevant cynomolgus macaques. Antagonizing IL-1 in mice with established infection reduced lung neutrophil numbers and partially restored the erythroid progenitor populations that are depleted by LZD. In macaques, we found no conclusive evidence of bone marrow suppression associated with LZD, indicating our treatment time may have been short enough to avoid the toxicities observed in humans. Though treatment was only 4 weeks (the FDA approved regimen at the time of study), we observed sterilization of the majority of granulomas regardless of co-administration of the FDA-approved IL-1 receptor antagonist (IL-1Rn), also known as Anakinra. However total lung inflammation was significantly reduced in macaques treated with IL-1Rn and LZD compared to LZD alone. Importantly, IL-1Rn administration did not impair the host response against Mtb or LZD efficacy in either animal model. Together, our data support that inhibition of IL-1 in combination with LZD has potential to be an effective HDT for TB and the need for further research in this area.

Introduction

Tuberculosis (TB) remains the top cause of death by a single infectious agent, with an estimated 10 million new cases of active TB and 1.3 million deaths in 2017 alone (1). Antibiotic treatment regimens are long and multi-drug resistant (MDR) and extensive-drug resistant (XDR) *Mycobacterium tuberculosis* (Mtb) strains have emerged, complicating treatment. Even those patients that are cured of the infection can suffer permanent deficits in lung function that result from inflammation and fibrosis (2). Host-directed therapies (HDTs) have been proposed as a potential option for improving therapy. Depending on the strategy, HDTs can function to enhance antimicrobial immune responses and shorten therapy, or inhibit pathological inflammation (3). Since HDTs would be used as part of a multi-drug regimen, targeting mechanisms that increase drug exposure or decrease toxicity are also possible. While some HDT strategies hold promise, very few have been rigorously tested in pre-clinical models (4).

Interleukin-1 (IL-1) has been implicated in TB disease severity and inflammation, making it a possible target of HDT. This cytokine plays an important yet complicated role in TB disease progression. The susceptibility of mice lacking critical mediators of IL-1 signaling indicates that initial production of IL-1 upon Mtb infection is essential for establishing protective immune responses necessary for disease control (5-8). In contrast, IL-1 production is regulated after the onset of adaptive immunity, via multiple mechanisms including IFNγ production(8), which acts via the induction of nitric oxide synthase 2 (NOS2)-dependent nitric oxide to inhibit IL-1β processing(9). Persistent IL-1 signaling can contribute to the accumulation of disease-promoting neutrophils in susceptible mice, and genetic variants that result in higher IL-1β production are associated with increased disease severity and neutrophil accumulation in humans (9-11). Given that HDT is designed to be administered to chronically infected patients

during treatment when persistent IL-1 production can play a pathological role, it could be beneficial to block the inflammation and disease promoting activities of this cytokine.

IL-1 may also play a role in the toxicity of linezolid (LZD), an increasingly important antibiotic for the treatment of drug-resistant TB, highlighted by its recent inclusion in a newly approved therapy for MDR-TB (12). While LZD has shown efficacy against XDR and MDR-TB, its wide-spread use has been limited by severe host toxicities that occur after more than 4 weeks of treatment (13, 14). Over the 6-20 month treatment course necessary to treat resistant TB, both reversible bone marrow suppression and irreversible neuropathies are common clinical manifestations (15). LZD-associated toxicities are generally attributed to the inhibition of mitochondrial translation and LZD-mediated bone marrow suppression is promoted by the subsequent mitochondrial damage. This damage acts on the NOD-like receptor family, pyrin domain containing 3 (NLRP3) protein that has been shown to be necessary for LZD-mediated bone marrow suppression in mice (16). NLRP3 forms an inflammasome complex containing caspase-1, which cleaves a number of substrates resulting in cell death and/or the release of active of IL-1β. While the importance of NLRP3 in bone marrow suppression is clear, the relative roles of inflammasome activation and IL-1 signaling remain uncertain.

Based on these studies, inhibiting the IL-1 pathway as a potential HDT could serve two purposes: first, to alleviate LZD-associated host toxicity and second, to reduce the pathology associated with unchecked IL-1 signaling during TB disease. Due to the pro-inflammatory nature of the IL-1 pathway, strict regulatory mechanisms exist within the host to quell this pathway. IL-1 receptor antagonist (IL-1Rn) is a protein produced constitutively at low levels that can increase in response to a variety of cytokine signals. IL-1Rn serves as a decoy ligand for the IL-1receptor type 1 (IL-1R1), blocking signal transduction and subduing activation of downstream pro-inflammatory pathways (17). Anakinra is an FDA-approved recombinant IL-

1Rn that is used to treat rheumatoid arthritis and other inflammatory disorders. As there are no FDA approved drugs to inhibit inflammasome activation, inhibition of the IL-1 pathway with biologics like Anakinra is currently the only feasible strategy to modulate this pathway in humans (18).

We hypothesized that the combination of Anakinra (herein referred to as IL-1Rn) with LZD for treatment of active TB disease would reduce LZD-associated toxicities and host inflammation. While there is little rationale to expect IL-1 blockade to enhance bacterial clearance by the antibiotic, suppression of both inflammation and LZD toxicity could provide a significant benefit. To test this concept, we employed two established TB animal models to assess differing aspects of host responses to LZD and IL-1R1 blockade. We used multiple strains of mice to model distinct disease states and dissect the relative importance of the inflammasome and IL-1 signaling in evaluating HDT efficacy. As a translational model, we used cynomolgus macaques in combination with [^{18}F] FDG PET CT serial imaging to track TB disease progression, including inflammation, before and during drug regimens (19). Cynomolgus macaques present a similar spectrum of Mtb infection as humans with pathology, granuloma structure and diversity, that recapitulates human TB (20-22). Importantly, we designed our study in macaques to reflect clinical standards, adhering to FDA guidelines for dosage and time frame of LZD and IL-1Rn administration. Together, our data indicate that IL-1 blockade alleviates LZD-mediated bone marrow (BM) suppression in mice and may accelerate the resolution of inflammation in both mice and macaques with TB.

Materials and Methods

Ethics Statement

All experimental manipulations, protocols, and care of the animals were approved by

the University of Pittsburgh School of Medicine Institutional Animal Care and Use Committee (IACUC). The protocol assurance number for our IACUC is A3187-01. Our specific protocol approval numbers for this project are 15117082, 16017370, 18124275, 13011368 and 16027525. The IACUC adheres to national guidelines established in the Animal Welfare Act (7 U.S.C. Sections 2131 - 2159) and the Guide for the Care and Use of Laboratory Animals (8th Edition) as mandated by the U.S. Public Health Service Policy.

All macaques used in this study were housed at the University of Pittsburgh in rooms with autonomously controlled temperature, humidity, and lighting. Animals were singly housed in caging at least 2 square meters that allowed visual and tactile contact with neighboring conspecifics. The macaques were fed twice daily with biscuits formulated for nonhuman primates, supplemented at least 4 days/week with large pieces of fresh fruits or vegetables. Animals had access to water *ad libitem*. Because our macaques were singly housed due to the infectious nature of these studies, an enhanced enrichment plan was designed and overseen by our nonhuman primate enrichment specialist. This plan has three components. First, species-specific behaviors are encouraged. All animals have access to toys and other manipulata, some of which will be filled with food treats (e.g. frozen fruit, peanut butter, etc.). These are rotated on a regular basis. Puzzle feeders foraging boards, and cardboard tubes containing small food items also are placed in the cage to stimulate foraging behaviors. Adjustable mirrors accessible to the animals stimulate interaction between animals. Second, routine interaction between humans and macaques are encouraged. These interactions occur daily and consist mainly of small food objects offered as enrichment and adhere

157 to established safety protocols. Animal caretakers are encouraged to interact with the
158 animals (by talking or with facial expressions) while performing tasks in the housing
159 area. Routine procedures (e.g. feeding, cage cleaning, etc) are done on a strict
160 schedule to allow the animals to acclimate to a routine daily schedule. Third, all
161 macaques are provided with a variety of visual and auditory stimulation. Housing areas
162 contain either radios or TV/video equipment that play cartoons or other formats
163 designed for children for at least 3 hours each day. The videos and radios are rotated
164 between animal rooms so that the same enrichment is not played repetitively for the
165 same group of animals.

166 All animals are checked at least twice daily to assess appetite, attitude, activity
167 level, hydration status, etc. Following *M. tuberculosis* infection, the animals are
168 monitored closely for evidence of disease (e.g., anorexia, weight loss, tachypnea,
169 dyspnea, coughing). Physical exams, including weights, are performed on a regular
170 basis. Animals are sedated prior to all veterinary procedures (e.g. blood draws, etc.)
171 using ketamine or other approved drugs. Regular PET/CT imaging is conducted on
172 most of our macaques following infection and has proved very useful for monitoring
173 disease progression. Our veterinary technicians monitor animals especially closely for
174 any signs of pain or distress. If any are noted, appropriate supportive care (e.g. dietary
175 supplementation, rehydration) and clinical treatments (analgesics) are given. Any
176 animal considered to have advanced disease or intractable pain or distress from any
177 cause is sedated with ketamine and then humanely euthanatized using sodium
178 pentobarbital.
179
180

Mice, infection and treatment

C57BL/6 (stock no. 000664), *Nos2*$^{-/-}$ (B6.129P2-Nos2^{tm1Lau}/J, stock no. 002609), C3HeB/FeJ (stock no. 00658), and *Nlrp3*$^{-/-}$ (B6.129S6-*Nlrp3*^{tm1Bhk}/J, stock no. 021302) were purchased from the Jackson Laboratory. Breeding pairs of Caspase-1/11 double knock out mice were kindly provided by Prof. Katherine Fitzgerald of the Department of Infectious Diseases at University of Massachusetts (UMASS) Medical School and bred in house. Mice were housed under specific pathogen-free conditions, and in accordance with the UMASS Medical School, IACUC guidelines. All mouse strains used in this study were of C57BL/6 background unless otherwise indicated.

The wild type strain of *M. tuberculosis* (Mtb) Erdman was used in these studies. Bacteria were cultured in 7H9 medium containing 0.05% Tween 80 and OADC enrichment (Becton Dickinson). For infections, mycobacteria were suspended in phosphate-buffered saline (PBS)-Tween 80 (0.05%); clumps were dissociated by sonication, and ~100 CFU were delivered via the respiratory route using an aerosol generation device (Glas-Col, Terre Haute, IN). At indicated time points mice were treated with 200mg/kg of Linezolid (LZD). These drugs were prepared in 0.5% carboxymethyl cellulose (CMC) and Polyethylene glycol 300 solution as the vehicle. Cohorts of mice were treated with anti-IL-1R1 antibody (InVivoMab, anti-mouse IL-1R, Clone JAMA147, BioXcell), either alone or in combination with LZD. 0.5% CMC and Polyethylene glycol was used as vehicle control. All antibiotic treatment was done by daily oral gavage. Anti-IL-1R1 (100ug/mouse/0.2mL) was administered every alternate day by subcutaneous and intraperitoneal route.

Macaque pharmacokinetic study and analytical method.

Uninfected macaques designated for other studies (n=3) were given 20mg/kg or 40mg/kg by oral gavage and plasma acquired at 0, 5, 19, 15, 20, 25 and 30 hours post LZD administration.

High pressure liquid chromatography coupled to tandem mass spectrometry (LC/MS-MS) analysis was performed on a Sciex Applied Biosystems Qtrap 4000 triple-quadrupole mass spectrometer coupled to an Agilent 1260 HPLC system to quantify LZD in macaque plasma. LZD chromatography was performed on an Agilent Zorbax SB-C8 column (2.1x30 mm; particle size, 3.5 µm) using a reverse phase gradient elution. Milli-Q deionized water with 0.1% formic acid was used for the aqueous mobile phase and 0.1% formic acid in acetonitrile for the organic mobile phase. Multiple-reaction monitoring (MRM) of parent/daughter transitions in electrospray positive-ionization mode was used to quantify the analytes. Sample analysis was accepted if the concentrations of the quality control samples were within 20% of the nominal concentration. Data processing was performed using Analyst software (version 1.6.2; Applied Biosystems Sciex).

Neat 1 mg/mL DMSO stocks for all compounds were serial diluted in 50/50 Acetonitrile water to create standard curves and quality control spiking solutions. 20 µL of neat spiking solutions were added to 20 µL of drug free plasma or control tissue homogenate, and extraction was performed by adding 180 µL of Acetonitrile/Methanol 50/50 protein precipitation solvent containing the internal standard (10 ng/mL verapamil & deuterated LZD-d3). Extracts were vortexed for 5 minutes and centrifuged at 4000 RPM for 5 minutes. 100 µL or supernatant was transferred for LC-MS/MS analysis and diluted with 100 µL of Milli-Q deionized water.

Rhesus macaque plasma (Lithium Heparin, Bioreclamation IVT, NY) was used as a surrogate to cynomolgus macaque plasma to build standard curves. LZD-d3 internal standard and verapamil were purchased from Toronto Research Chemical. The lower and upper limits of quantitation (LLOQ and ULOQ) were 1 ng/mL and 50,000 ng/mL respectively. The following MRM transitions were used for LZD (338.00/235.00), LZD-d3(341.20/297.20), and verapamil (455.40/165.20).

Macaques, infection and treatment

All housing, care, and experimental procedures were approved by the University of Pittsburgh School of Medicine Institutional Animal Care and Use Committee (IACUC). Examination of animals was performed in quarantine to assess physical health and confirmation of no previous *M. tuberculosis* infections as previously described (23). Cynomolgus macaques (*Macaca fascicularis*) (N=10) were purchased for this study from (Valley Biosystems). Bone marrow control (non-drug treated) samples were taken from Mtb-infected cynomolgus macaques in unrelated ongoing studies (N=5). For the current study, all 10 animals were infected bronchoscopically with 12 CFU of Mtb strain Erdman. After active disease developed (3-5 months), NHPs were randomized to LZD only (N=5) or LZD+IL-1Rn (N=5) treatment groups. For randomization, macaques were paired based on total FDG activity in lungs (a surrogate for total thoracic CFU), and then assigned to treatment by coin flip (20). LZD was administered twice a day orally with food (30mg/kg), while IL1-Rn was given at 2mg/kg once each day by subcutaneous injection. All animal data are provided in Supplementary Table 1. Medication compliancy was monitored at every administration and pharmacokinetic analysis performed at select times. Drug treatments were administered for 4 weeks prior to necropsy. Bronchoalveolar lavages (BAL) were performed prior to drug-treatment and 3 weeks-post start of treatment for CFU, flow cytometry and multiplex assays.

Macaque PET/CT Imaging

Positron emission tomography (PET) with computed tomography (CT) imaging was performed with 2-deoxy-2-[^{18}F]-D-deoxyglucose (FDG) throughout the study as previously described (19). Serial scans were performed throughout the study to track disease progression and changes during drug treatment. Total FDG activity of the lungs was measured over the course of infection and drug treatment as previously described (19). Granulomas identified on scans were denoted, measured (mm) and standard uptake values (SUVR) were determined to assess metabolic activity, a readout for inflammation. SUVR values were normalized to muscle and

SUVR and size measurements were determined at each scan over time to compare pre-and post-drug treatment. Each animal was scanned prior to necropsy to identify granulomas for matching at necropsy; granulomas $\geq$ 1mm are distinguishable by PET/CT.

Macaque Necropsy

Necropsies were performed as previously described. In short, multiple tissues (granulomas, lung lobes, thoracic lymph nodes, peripheral lymph nodes, liver, spleen, bone marrow) were excised and homogenized into single-cell suspensions for assessment of bacterial burden and immunological assays. Granulomas were individually excised (PET/CT identified and others not identified on scans) and split (size permitting) with one-half for homogenization and single cell suspension and the other half processed for histological analysis. Bone marrow samples were obtained from the sternum, with a portion sent for histological analysis while single cell suspensions were acquired as previously described (24). Bacterial burden was assessed from each tissue by plating serial dilutions on 7H11 agar plates and incubated at 37°C in 5% CO_2 for 21 days before enumeration of Mtb CFU.

Flow cytometry and Immunoassays

Mice. Single cell suspensions were prepared from the infected mouse organs. Briefly, lung tissue was digested with Collagenase type IV/DNaseI and passed through 40 μm cell strainers to obtain single cell suspension. Red blood cells were lysed using Tris-buffered Ammonium Chloride (ACT) Non-specific antibody binding sites were blocked by Fc-Block CD16/32 (Clone 93, cat. no. 101319) and the cells were stained with anti-CD3-PE (Clone 17A2, cat. no. 100205), anti-CD11b-PerCP Cy5.5 (Clone M1/70, cat. no.101227), anti-Ly-6G-FITC (Clone 1A8, cat. no.127605), anti-Ly-6C-PE (Clone HK1.4, cat. no.128007), anti-Gr1-APC (Clone RB6-8C5, cat. no.108411), anti-Ter119-PE (Clone TER119, cat. no.116208), anti-CD71-FITC (clone

RI7217, cat. no. 113806). Antibodies were purchased from BioLegend. All analyses were performed on live cells only after staining them with fixable live dead stain conjugated with eFlour780, purchased from eBiosciences. All the staining was done according to the manufacturer's instructions. Lung, spleen and bone marrow cells were surface stained for 30 minutes at room temperature, fixed for 20 minutes at 4^0C using the Cytofix buffer (BD-Biosciences, cat. no. 554655). Data were acquired in a BD LSRII flow cytometer in the flow cytometry core facility at UMASS medical school and analyzed with FlowJo Software (Treestar, Inc.). Gating strategies are provided in applicable figures.

Macaques. Single cell suspensions acquired from homogenization of granulomas, lung lobes and lymph nodes were subjected to intracellular cytokine staining (ICS). Prior to staining, cells were incubated in RPMI 1640 containing 1% HEPES, 1% L-glutamine, 10% human AB serum, and 0.1% brefeldin A (Golgiplug; BD Biosciences) for 3 h at 37°C in 5% CO_2. After viability staining (Invitrogen), surface antigens and intracellular cytokines were assessed using standard protocols. Surface markers include CD3 (SP34-2; BD Pharmingen), CD4 (L200; BD Horizon), CD8 (RPA-T8; BD Horizon) for T cells and CD11b (ICRF44; BD Pharmingen), CD206 (19.2; BE Pharmingen) for macrophages/neutrophils. Calprotectin (27E10; ThermoFisher) was stained intracellularly to identify neutrophils. For bone marrow, single cell suspensions underwent red blood cell lysis (BD Pharm Lyse) before incubation in alpha-MEM + 10% Stasis™ FBS (Gemini Bio-Products) + MitoTracker™ Red CMXRos (Invitrogen) for 30 minutes to stain for membrane potential of mitochondria. Cells were then stained for viability (Invitrogen) and surface stained to distinguish erythroid progenitor populations by CD34 (581; Biolegend), CD235a (HIR2; BD Pharmingen), CD71 (L01.1; BD Pharmingen) and CD45 (D058-1283; BD Pharmingen). All samples were acquired on an LSR II (BD) and analyzed with FlowJo Software (Treestar, Inc.). Gating strategies are provided in applicable figures.

For the multiplex assays, all samples and supernatants were stored at -80°C from time of necropsy until time of assay. Five representative granuloma supernatants were randomly

selected from each animal using JMP Pro v12 (SAS Institute Inc.). Supernatants were thawed and filtered with a 0.22uM syringe filter to remove infectious bacteria and debris, then kept on ice throughout the assay. For BAL samples, supernatants were concentrated using regenerated cellulose centrifugal filter tubes (3,000 NMWL, Millipore Sigma) to a final 10X concentration (5mL to 0.5mL). Both granuloma and BAL supernatants were evaluated with a ProcartaPlex multiplex immunoassay (Invitrogen) that assesses thirty cytokines and chemokines specific for NHPs. We followed the manufacturer's protocol with one modification in which we diluted the standard out an extra dilution to increase the range of detection. Results were analyzed by a BioPlex reader (BioRad).

Histopathology and immunofluorescence

Mice. Lung tissues were fixed in 10% buffered formalin and embedded in paraffin. Five micrometer-thick sections were stained with hematoxylin and eosin (H&E). Tissue staining was done by the Diabetes and Endocrinology Research Center histopathology core facility at the University of Massachusetts Medical School or immunology core facility of Albany medical college, NY. Brightfield images were acquired in Abaxis VETSCAN HD microscope.

Paraffin embedded lung tissue sections were cut at 5 µm thickness, mounted on ultraclean glass slides covered in silane, deparaffinized, then dehydrated and rehydrated using the following steps: Ethanol solutions (30, 50, 70, 90, 95 and 100 % for 3 min each), xylenes (2 different solutions for 10 min each) and ethanol solutions (100, 95, 90, 70, 50 and 30 for 3 min each). The slides were washed once in Tris buffer saline (TBS) for 5 min. Slices were subjected to antigen retrieval by boiling in sodium citrate buffer at pH=6.0 for 20 min and incubated in 0.1% Triton-X 100 for 5 min. Slices were removed and allowed to equilibrate to room temperature for at least 20 min and rinsed with distilled water. Tissue sections were blocked (blocking solution; 0.5 M EDTA, 1% BSA, in PBS) and incubated overnight in primary antibodies against the proteins related to our studies. Sections were stained for nuclei (DAPI, blue

staining), anti-mouse CD3e (cat.no. ab16669, green staining), anti-mouse Ly-6G (clone 1A8, cat. no. 127602) to identify neutrophil granulocytes (Cy3, red staining). As controls, pre-immune serum and isotype matched controls were used. After incubation, the tissues were washed several times with sterile TBS at room temperature and incubated in the respective secondary antibodies (anti-rabbit conjugated to Alexa-488, anti-rat conjugated to Cy3) for at least 2h at room temperature. Tissue sections were mounted using Prolong Gold Antifade reagent (Invitrogen, grand Island, NY) with DAPI, and the tissue sections were examined in ECHO Revolve 4 microscope. Isotype matched control antibodies were used for checking antibody specificity.

Macaques. As previously described, samples acquired at necropsy were formalin fixed, paraffin embedded, cut into ~5µm serial sections and stained with H&E (23). A study-blinded veterinary pathologist assessed and characterized each granuloma, indicating size, type, distribution and cellular composition. Sterna for bone marrow analysis were excised and formalin fixed then transected longitudinally into 1 to 2 sternebral unites and placed in Cal-Ex Hydrochloric acid decalcification solution for 2-4 hours. Upon removal, specimens were washed and trimmed to test for adequate mineral removal, then submitted for routine tissue processing with other tissue specimens as described above.

Statistical Analysis

Mouse studies: Equal variance between samples was assessed by Brown-Forsythe test. Experiments in which variances were equivalent were analyzed by one-way ANOVA with Sidak's multiple comparisons test. Those with unequal variances were analyzed by Welch ANOVA and Dunnett's multiple comparisons test. P values < 0.05 was considered significant.

Macaque studies: Nonparametric U tests (Mann-Whitney) were performed for two-group comparisons and Kruskal-Wallis tests were performed for three-group comparisons as indicated on data sets with non-normal distributions. Wilcoxon signed rank tests were performed for

matched pairs. Fisher's exact test was run on any categorical data. P values < 0.05 were considered significant. Total lung FDG activity was $\log_{10}$-transformed. Note that for any log-transformed data, a $\log_{10}(x + 1)$ transform was implemented so that zeroes were not excluded from the graphs or analyses. A two-way ANOVA was utilized to test whether treatment or time (or an interaction between these factors) had an effect on total lung inflammation. Time was found to be a statistically significant effect (p=0.0046); therefore, Dunnett's multiple comparison tests were then used to compare each time point to pre-drug treatment within each treatment group. For bivariate data, a linear regression was used to test the linear relationship between the variables and the R^2 and p-value for the F-test are reported in the accompanying figure legend. Statistical analyses were performed in GraphPad Prism 8 (GraphPad Software, San Diego, CA). A regression equation created from control animals from previous studies was used to create a 95% prediction interval for total thoracic bacterial burden using total lung FDG activity on the scan just before drug treatment (20). The lower and upper bounds and the mean of this prediction interval were subtracted from each animal's total CFU to estimate change in CFU over the course drug treatment. All statistical analyses are referenced in the corresponding figure legends.

Results

IL-1 receptor blockade reduces inflammation in mouse models of TB disease.

Given the complex role played by IL-1 during TB, we initially sought to determine the effect of inhibiting this cytokine during TB disease in mice. We used a blocking antibody to the murine IL-1 receptor type 1 (αIL-1R1) since this reagent has been shown to alter TB disease in mice (25), and we previously found that recombinant human IL-1Rn (Anakinra) has little effect in this mouse model. Two mouse strains were employed to assess the effects of these treatments in

387 animals with different amounts of IL-1 activity. In relatively resistant C57BL/6 animals, mature
388 IL-1 production is controlled by IFNγ-dependent nitric oxide production, whereas unregulated IL-
389 1 drives inflammatory disease characterized by increased number of neutrophils (PMNs),
390 bacterial burden (CFU) in the lungs and significant weight loss observed in Mtb-infected *Nos2*$^{-/-}$
391 mice that lack this regulatory pathway (9, 10).
392 αIL-1R1 was administered to the animals between days 14 and 28 post infection after the onset
393 of adaptive immunity. In both resistant (C57BL/6) and susceptible (Nos2$^{-/-}$) mice, αIL-1R1
394 treatment significantly reduced PMN numbers in the lungs. In addition, this treatment reversed
395 the weight loss observed in *Nos2*$^{-/-}$ animals (Fig. 1A-B). Somewhat surprisingly, this regimen
396 also modestly reduced the mean bacterial burden in lungs and spleens, with this reduction
397 meeting statistical significance in the spleens of *Nos2*$^{-/-}$ mice (Fig. 1C-D). This generally
398 beneficial effect of αIL-1R1 treatment was consistent with qualitatively improved
399 histopathological disease (Fig. 1E). By no metric did this αIL-1R1 treatment exacerbate disease
400 in either mouse strain.
401
402 **IL-1 blockade alleviates lung inflammation and hematopoietic suppression during LZD**
403 **treatment in mice.**
404 The IL-1R1 blocking antibody was next tested in combination with LZD to determine whether the
405 efficacy or toxicity of the antibiotic was altered. C3HeB/FeJ mice, which are relatively
406 susceptible to Mtb and develop histopathological lesions that more closely resemble human
407 disease, were used for these studies. To model established disease, mice were treated
408 between days 28 and 46 post-infection with vehicle alone, LZD, αIL-1R1 or a combination of the
409 two. As previously reported, LZD was effective in this model, reducing lung neutrophil numbers,
410 bacterial burden and weight loss (Fig. 2 A-D) (26). The addition of αIL-1R1 to this regimen
411 further reduced lung neutrophil numbers. IL-1 blockade had very little effect on bacterial

412 burdens in lung or spleen, whether given alone or in conjunction with LZD. The mean CFU
413 burden in αIL-1R1-treated animals was within 2.3-fold of the untreated groups, and only the αIL-
414 1R1-associated decrease in the spleens of LZD treated animals approached significance. As
415 IL-1β production in response to both Mtb infection (9) and LZD treatment (16) depends largely
416 on the NLRP3 inflammasome, we also investigated a regimen in which LZD and a small
417 molecule NLRP3 inhibitor (MCC950) was administered between days 56 and 77 post-infection.
418 As observed with αIL-1R1, the addition of MCC950 reduced PMN numbers in the lung, relative
419 to LZD alone, and did not significantly alter bacterial killing (Fig. 2 E-G). Using a more rapid
420 treatment protocol and C57BL/6 mice with genetic deficiencies in Caspase 1 or NLRP3, we
421 confirmed that the antimicrobial activity of LZD was unaffected by inflammasome activation
422 (Supplementary Fig. 1A-D). Mice were treated between days 14 and 28 post-infection and the
423 effect of LZD on bacterial burden and lung neutrophil number was at least as large in the
424 knockout animals as the wild type controls.
425
426 Next, we evaluated the hematopoietic suppression caused due to LZD treatment in the bone
427 marrow and spleens of C3HeB/FeJ mice. In small animals, bone marrow serves as the primary
428 site of hematopoiesis, but during infection or stress, the spleen functions as an extramedullary
429 hematopoietic organ to compensate for the increasing demand of blood cells in the
430 periphery(27). As LZD did not alter the myeloid cells in the bone marrow (data not shown), and
431 previous reports have shown its effects on erythropoiesis (16), we investigated the effect of this
432 oxazolidinone on erythroid lineage cells in both these organs. Using flow cytometry, erythroid
433 progenitors can be divided into a progression of precursors: pro-erythrocyte (ProE), EryA, EryB,
434 and EryC (Fig. 3A). These populations were quantified in each tissue of Mtb-infected animals
435 treated with LZD and/or αIL-1R1. In both bone marrow and spleen, LZD had a profound effect,
436 nearly eliminating early erythroid progenitors of the ProE, EryA and EryB classes (Fig. 3B-E).

Simultaneous treatment with αIL-1R1 largely reversed the effect of LZD in the spleen, restoring these immature precursors to approximately half of their untreated levels. While αIL-1R1 also significantly increased the number of erythroid precursors in the BM, the suppression of LZD toxicity was less pronounced at this site.

In sum, studies in the mouse model indicated that the addition of αIL-1R1 to an LZD regimen could reduce the number of lungs PMN and ameliorate hematopoietic toxicity, while not compromising antimicrobial activity. These observations justified further studies in a non-human primate model.

Changes in TB disease in macaques treated with LZD and HDT by PET/CT

Previously we published the efficacy and pharmacokinetics of LZD in cynomolgus macaques treated for 8 weeks with a single daily dose of 30 mg/kg (14). To adhere to FDA guidelines for LZD administration at the time we initiated this study and reproduce clinical exposure at 600 mg twice daily (b.i.d.), we shortened treatment duration to 4 weeks and increased the dosing frequency to 30 mg/kg b.i.d. Dose finding studies were carried out in uninfected cynomolgus macaques to ensure that adequate drug concentrations similar to those achieved in patients at 600 mg b.i.d. were reached in the blood (Supplementary Fig. 2).

To assess this LZD regimen and HDT with IL-1Rn, we infected 10 cynomolgus macaques with Mtb strain Erdman and monitored development of active TB disease (Supplementary Table 1 and Supplementary Fig. 2). Infected macaques were then randomized to a 4-week drug regimen of LZD (n=5) or LZD+IL-1Rn (n=5) (Supplementary Fig. 2). Our model has the advantage of tracking disease progression throughout infection and treatment using serial ^{18}F-FDG PET CT scans (14, 28). Lung inflammation quantified by total FDG activity in the lungs is

462 correlated with total thoracic bacterial burden as previously described (19). Here we quantified
463 total lung FDG activity before and during treatment. 3D rendered images provide a visual for
464 changes in overall lung inflammation in the “best” and “worst” animals for both treatment groups
465 (Fig. 4A). Quantification of total lung FDG showed no significant difference in inflammation at
466 time of necropsy between LZD and LZD+IL-1Rn treatment groups (Fig. 4B), however a slight
467 change in slope with IL-1Rn treatment was observed. To expand on this finding and test if
468 LZD+IL-1Rn reduced total lung FDG activity more effectively than LZD alone over time, we
469 compared the change in FDG activity between 0, 2 and 4 weeks post treatment. In LZD only
470 treated macaques, there was no significant decrease in total lung FDG activity after 2
471 (p=0.0857) and 4 weeks of treatment (p=0.2876) (Fig. 4B). In contrast, LZD+IL-1Rn treatment
472 resulted in a significant reduction in total lung FDG activity after 2 and 4 weeks (p=0.0242,
473 p=0.0237 respectively). To assess whether these changes in lung inflammation were reflected
474 in individual granulomas, we used PET CT scans acquired pre-treatment and at 4 weeks post-
475 treatment to determine changes in granuloma physical size (mm) and metabolic activity as
476 Standard Uptake Value (SUVR) of FDG per granuloma (Fig. 4C-D) (19). SUVR indicates the
477 inflammatory state of each individual granuloma, allowing us to track specific lesions throughout
478 treatment for changes in activity. After treatment, while the majority of granulomas decreased in
479 size and SUVR, there was variability within an animal and between animals and no significant
480 differences between LZD and LZD+IL1-Rn treated animals. These data indicate that blocking of
481 IL-1R in combination with LZD reduces total lung inflammation more efficiently than LZD alone.
482
483 **Addition of IL-1Rn does not alter LZD bacterial clearance**
484 IL-1Rn does not have direct bactericidal activity, therefore addition of IL-1Rn to LZD treatment
485 should not directly influence bacterial killing and burden. However, to ensure
486 immunomodulation with IL-1Rn did not have detrimental effects on host antibacterial immune
487 responses, we performed comprehensive bacterial burden analysis at necropsy as previously

488 described (20). In short, we acquired individual granulomas identified by PET CT as well as
489 other TB pathologies, thoracic lymph nodes, uninvolved lung tissue and extrapulmonary lesions
490 for bacterial plating and CFU determination. Total thoracic CFU (lung + lymph nodes) was not
491 significantly different between LZD and LZD + IL-1Rn in macaques ($p = 0.1508$). Similarly,
492 separate analysis of lung CFU excluding thoracic lymph nodes did not demonstrate significant
493 differences between groups ($p=0.5476$) (Fig. 5A). We did not have untreated control macaques
494 available in this study, therefore we provide total thoracic CFU for 3 historical control animals
495 that were similarly infected and necropsied at a similar time point; these data serve as reference
496 for expected CFU at this time point and were not included in statistical analyses. While the
497 treatment groups had similar frequencies of sterilized granulomas (LZD = 68.42%, LZD+IL-1Rn
498 = 72.22%), it is important to note that the majority of granulomas were sterilized during the short
499 four-week course of LZD or LZD+IL-1Rn treatment. We previously reported that a 2-month
500 lower dose regimen of LZD could reduce bacterial burden compared to untreated controls, with
501 ~80% sterilized granulomas in treated animals and ~20% sterilized in untreated (14). This
502 supports that high dose LZD as a single drug is effective at killing bacteria even in a short (4
503 week) regimen. The lymph nodes are a recently identified reservoir for Mtb and a hub for
504 immune cell interactions (29), therefore we assessed HDT effects on bacterial burden in
505 thoracic lymph nodes after treatment. We saw no significant difference in overall lymph node
506 CFU nor CFU per lymph node (Fig. 5C), indicating addition of IL-1Rn did not measurably alter
507 LZD efficacy or antibacterial immunity in lymph nodes. To better understand the efficacy of high
508 dose LZD for 4 weeks, we estimated the pre-treatment total thoracic CFU for each macaque
509 using the total lung FDG by PET CT as previously described (20), and compared the true
510 bacterial burden post-treatment against the estimated pre-treatment value. This analysis allows
511 us to estimate the magnitude of LZD bacterial killing during LZD and LZD+IL-1Rn treatment. All
512 macaques had lower total thoracic CFU at necropsy compared to the estimated total thoracic
513 CFU prior to treatment start and on average the total CFU was ~100-fold lower than estimated

514 CFU prior to treatment (Fig. 5D). Our data indicate that while IL-1Rn did not significantly
515 enhance bacterial killing, it did not impair LZD-mediated bacterial clearance, an important
516 observation for HDT development.
517
518 **Lack of LZD-induced bone marrow suppression in macaques**
519 In humans, LZD is associated with host toxicities during extended treatment periods of greater
520 than 4 weeks (30) resulting in the FDA limitation of LZD to less than 4 weeks for most
521 indications. We designed our study in macaques to follow FDA-guidelines for transition to
522 possible human trials, therefore the potential for bone marrow toxicity to occur within this
523 timeframe in macaques was unknown. To determine whether bone marrow suppression
524 occurred during the 4-week high dose LZD therapy and whether IL-1Rn could modulate any
525 observable host toxicities, we isolated bone marrow at necropsy from the sternum of each
526 macaque and assessed erythropoietic progenitor populations and mitochondrial function by flow
527 cytometry (Fig. 6A). During homeostatic erythropoiesis, a 1:8 ratio is maintained between ProE
528 and EryC progenitor populations. Changes in this ratio can be used to indicate disruption of
529 erythropoiesis. In macaques, there was no significant difference in ProE:EryC ratios between
530 the treatment groups (Fig. 6B). We also analyzed control bone marrow from untreated Mtb-
531 infected macaques involved in other on-going studies (TB only), which showed no significant
532 difference between ProE:EryC ratios compared to treatment groups. To determine whether LZD
533 was affecting mitochondrial function, we stained bone marrow cells with MitoTracker™ Red
534 CMXRos which only stains mitochondria with active membrane potential, indicating function of
535 those organelles (Fig. 6B). Regardless of treatment, the MitoTracker MFI remained similar,
536 indicating that mitochondrial function is the same among groups. To confirm our observations,
537 a pathologist evaluated bone marrow tissue sections and found no observable differences
538 between TB only, LZD and LZD+IL-1Rn groups in terms of cellularity (myeloid:erythroid ratios)
539 or abnormalities (Fig. 6C). We could not consistently identify progenitor populations in blood or

spleen, therefore we performed complete blood counts (CBCs) during treatment to identify signs of bone marrow suppression (i.e., anemia, thrombocytopenia). There were no observable differences between LZD and LZD+IL-1Rn treatments (Supplementary Fig. 3). In conclusion, 4 weeks of LZD was not sufficient to induce observable bone marrow suppression in cynomolgus macaques and blocking of IL-1R did not alter bone marrow status during LZD treatment of TB.

Reduction in neutrophil signatures in the lung during treatment

To determine whether addition of IL-1Rn to LZD treatment modulated immune populations similar to observations in the mouse model, bronchoalveolar lavages (BAL) were acquired prior to the start of treatment and 3 weeks post treatment. Innate and adaptive immune cell populations were identified and frequencies were assessed by flow cytometry (Fig. 7A). Population frequencies of CD4 T cells, CD8 T cells, neutrophils (PMNs) and macrophages remain similar between LZD or LZD+IL-1Rn, indicating that IL-1Rn did not significantly alter the frequencies of immune populations in the airways. However, we observed a possible reduction in neutrophils post treatment in both groups. Therefore we pooled LZD and LZD+IL-1Rn treated animals and compared pre and post treatment immune populations. Although macrophage populations were relatively unchanged, there was a significant reduction in neutrophil frequency in the BAL after 3 weeks of treatment with LZD, regardless of IL-1Rn ($p=0.0098$). To determine whether the cytokine milieu in the airways changed during treatment, a subset of 3 animals per group were chosen at random for analysis by multi-plex using 10X concentrated BAL fluid (Fig. 7B). Statistical analysis was performed on combined treatment groups to only compare pre- and post-treatment changes. We assessed IL-1β and IL-1RA and saw no significant changes after treatment (IL-1β $p=0.1562$, IL-1RA $p=0.1250$). Interferon-inducible T cell alpha chemoattractant (I-TAC) is upregulated in response in interferons and IL-1 and is generally an indicator of inflammation, which appeared to be reduced post treatment, however was not

565 statistically significant (p=0.0625). IL-8, a neutrophil chemoattractant, was significantly reduced
566 after treatment, mirroring the reduction in neutrophil frequency observed by flow cytometry and
567 the mouse data. These data suggest that treatment with either LZD or LZD+IL-1Rn rapidly
568 reduces inflammatory signatures associated with TB disease in the airways.
569
570 **IL-1 blockade modulates granuloma environment and pathology**
571 To determine whether IL-1Rn modulated immune responses at the site of infection, we chose at
572 random 5 granulomas per animal (25 per treatment group) and performed a multi-plex analysis
573 of granuloma supernatants (Fig. 8A). There were no significant differences in IL-1β, IL-1RA, or
574 IL-18 levels in either treatment group. IL-2 and IL-17 are correlated with protective immune
575 responses during TB (31) and while IL-2 levels in LZD+IL-1Rn treatment were not statistically
576 higher (p=0.0882), a statistically significant increase in IL-17a in LZD+IL-1Rn treated animals
577 was observed. Interestingly, G-CSF/CSF-3 levels were also significantly higher in LZD+IL-1Rn
578 treated granulomas (p=0.0004). These results indicate IL-1Rn immune modulation occurs in
579 the granuloma environment. While we did not see a significant difference in granuloma
580 inflammation by SUVR between treatment groups (Fig 4C), we questioned whether the changes
581 in cytokines could be associated with change in SUVR. Therefore, we performed linear
582 regression analyses and found a positive correlation between IL-1β and fold change of SUVR in
583 LZD+IL-1Rn granulomas (Fig 8B). The IL-1 pathway is associated with fibrosis, which
584 increases in granulomas during drug treatment (32). Furthermore, IL-17 and G-CSF are also
585 associated with fibrosis (33). To determine whether immunomodulation by IL-1Rn changed
586 granuloma pathology, granulomas suitable for histological analysis were evaluated by a study
587 blinded pathologist and lesions were categorized based on treatment groups and descriptive
588 qualities (Fig. 8C). Of lesions acquired from LZD only animals, ~71% were identified as fibrotic
589 (n= 40/56), while those treated with LZD+IL-1Rn had ~85% fibrotic lesions (n=39/46) with no

significant difference in frequency of fibrotic lesions between treatment groups. We also compared the frequency of granulomas that were deemed necrotizing or non-necrotizing ("other" indicates neither categorization). Granulomas from LZD+IL-1Rn treated animals had significantly more non-necrotizing granulomas (~74%, n=34/46), compared to those from LZD alone treated macaques (~46%, n=26/56). The proportion of necrotizing granulomas was significantly lower in the LZD+IL-1Rn treatment group (13.04%, n=6/56) compared to LZD alone (30.36%, n=17/56) (p=0.0151). These data suggest that addition of IL-1Rn influences inflammation and antibiotic-associated pathology dynamics of granulomas.

Discussion

HDTs are a tantalizing solution to improve TB therapy, however the complexities of host-pathogen interactions and host variability call for rigorous pre-clinical testing before implementation in humans. Here, we sought to determine the efficacy and safety of an HDT for TB comprised of LZD and IL-1Rn. IL-1 plays a complex role during TB, as IL-1 is important for early control of infection (7, 8, 34-36), yet is also associated with pathology at later times(10, 11). To validate the safety of IL-1Rn in this context, we first assessed the effects of IL-1 inhibition on TB disease progression in mice, using treatment regimens designed to concentrate on established disease. In C57BL/6, Nos2$^{-/-}$ and C3HeB/FeJ mice, αIL-1R1 blockade reduced PMN infiltrates that are associated with pathological inflammation and did not impair bacterial control. The effect on bacterial control differs from a recent report in which lung bacterial burdens were increased by a similar αIL-1R1 treatment in C57BL/6 or C57BL/6 animals carrying the super susceptibility to tuberculosis-1 (Sst1) allele(25). We hypothesize that these differences are related to the timing of treatment, relative to the onset of adaptive

614 immunity. Once infection is established, bacterial control is mediated predominantly via
615 T cell functions, potentially reducing the importance of IL-1 dependent mechanisms(37).
616 According to this model, the effect of IL-1 inhibition will depend on the timing of
617 administration, as well as experimental factors that alter the timing of T cell priming and
618 expansion, such as bacterial strain and dose. Regardless, our data indicate that IL-1
619 blockade can be beneficial in the context of established disease.
620
621 Any HDT will be administered in conjunction with antimicrobial therapy. When co-
622 administered with LZD, blockade of IL-1R1 reduced PMN infiltrates in the mouse
623 models, compared to the antibiotic alone. In macaques, IL-1Rn in conjunction with LZD
624 significantly reduced overall lung inflammation as assessed by PET CT while LZD alone
625 was more variable. IL-1Rn did not significantly enhance bacterial clearance compared
626 to LZD alone, which was not surprising as we did not expect IL-1Rn to have direct
627 antibacterial functions. However, it was important to assess bacterial burden during IL-
628 1Rn treatment to ensure IL-1 blockade did not modulate host-mediated antibacterial
629 mechanisms in granulomas and lymph nodes. In CFU positive lymph nodes, we
630 observed a slight reduction in bacterial burden with IL-1Rn that approached significance
631 ($p=0.0965$). Further studies should include assessing the influence of drug treatment
632 and immunomodulation in lymph nodes, as thoracic lymph nodes are recognized as a
633 site of Mtb persistence (29)
634
635 To further assess the effects of IL-1Rn modulation of immune responses, we observed
636 a decrease in neutrophils (PMNs) and a corresponding decrease in IL-8 in the airways

637 of both treatment group (LZD or LZD+IL-1Rn). This indicated LZD alone was
638 efficacious in reducing PMN inflammatory signatures, likely due to the reduction in
639 bacterial burden. In granulomas, levels of IL-1β, IL-1RA and IL-18 were not affected by
640 IL-1Rn treatment in the subset examined. As IL-1Rn does not affect inflammasome
641 formation and function it is not surprising that IL-1β and IL-18 production were minimally
642 modulated by IL-1Rn. IL-1RA levels remained unchanged between treatment groups,
643 which could be due to our method of detection or kinetics of consumption. Our
644 multiplex analysis is specific for non-human primates and may not recognize
645 recombinant human IL-1RA like Anakinra. In LZD+IL-1Rn treated granulomas we found
646 a strong positive correlation between IL-1β levels and fold-change in SUVR, a surrogate
647 for inflammation. These data highlight the relationship between IL-1β and inflammation
648 in granulomas, further supporting the potential of IL-1 blockade as an HDT. In TB, IL-2
649 and IL-17A have protective functions however are primarily expressed by T cells (31).
650 While IL-1β has been reported to enhance IL-17A production by T cells in mice, these
651 studies have primarily used model-antigen systems and may not reflect a chronic
652 infection like TB (38). IL-1 exacerbates pathology later in TB infection, indicating the
653 effects of IL-1 on adaptive immunity are complex and likely dependent on the host
654 system and infection model being used. G-CSF was increased in granulomas from
655 LZD+IL-1Rn treated macaques which, combined with our observations of reduced PMN
656 infiltrates in mouse lungs and macaque airways, indicates a paradoxical role of G-CSF
657 as a neutrophil differentiation factor (39). However, in a model of LPS-induced lung
658 injury G-CSF blockade induced accumulation of PMNs and increased inflammation in

659 the lungs, indicating pulmonary inflammation may not follow dogmatic rules of canonical
660 inflammatory pathways (39).
661
662 Lung fibrosis is modulated by the IL-1 pathway and while fibrosis is associated with
663 healing tissue, lung fibrosis can cause secondary complications after TB disease
664 resolution (2). We have shown in previous studies that TB drug therapy induces fibrosis
665 in granulomas (32, 40). These studies in combination with the correlation between IL-1β
666 and SUVR led us to assess whether LZD+IL-1Rn was associated with changes in
667 granuloma pathology. While we did not observe a difference in fibrosis, there was a
668 significant decrease in frequency of necrotizing granulomas with IL-1Rn in addition to
669 LZD therapy. Thus, while there is no synergistic effect between IL-1Rn and LZD in
670 promoting fibrosis associated with drug clearance, the reduction in neutrophils observed
671 in mice and macaques could skew granuloma resolution towards a non-necrotizing
672 lesion (41). Further studies with IL-1Rn alone could elucidate these dynamics, however
673 we designed this macaque study with intention to be translatable to humans. We could
674 not justify an IL-1Rn only treated group as TB-patients would receive anti-microbial
675 therapy with any HDT or immunomodulatory intervention. However, our findings give
676 precedence for further exploration of the potential of IL-1Rn as an HDT for TB and will
677 require additional studies to determine mechanism and safety.
678
679 Our second goal was to abrogate LZD-associated bone marrow suppression with IL-
680 1Rn therapy, thereby increasing the efficacy and therapy potential of LZD in TB. While
681 we designed our HDT to match the current FDA guidelines for LZD and IL-1Rn

682 schedules, this resulted in a lack of observable bone marrow suppression in macaques.
683 In mice however, LZD-induced bone marrow suppression was reduced with the addition
684 of IL-1R1 antagonist, supporting our initial hypothesis of the therapeutic potential of IL-
685 1Rn in reducing LZD toxicity. The role of IL-1 signaling is consistent with the ability of IL-
686 1 to suppress erythropoiesis in mice by reducing the number of progenitors (42). The
687 remaining deficit in erythropoiesis during IL-1 blockade could reflect either incomplete
688 inhibition by IL-1Rn or an independent role of inflammasome activation. Optimizing this
689 effect will require further work to understand the relative roles of IL-1 signaling and
690 inflammasome activation.
691
692 Overall, our data support previous findings in macaques that LZD has superb efficacy
693 against TB, administered here as a single-drug given for only 4-weeks, supporting LZD
694 as an antimicrobial for MDR/XDR-TB cases (12). IL-1Rn therapy in conjunction with
695 LZD was successful in reducing TB-associated inflammation with no negative effects on
696 bacterial clearance. The differences in bone marrow suppression between mice and
697 macaques highlights the importance of assessing HDTs in multiple models prior to
698 human trials, as there are clear biological differences between the two models.
699 Anakinra (IL-1Rn) is already FDA-approved for adult and pediatric treatment of other
700 inflammatory disorders and our data provide pre-clinical evidence for IL-1Rn
701 consideration as potential therapy in TB. Further safety and mechanism assessments
702 in translatable animal models are required, but one could envision IL-1Rn therapy to
703 limit destructive inflammation for severe cases of TB. While our study emphasizes the
704 importance of rigorous testing of HDTs for TB in multiple translational models prior to

implementation in human trials, we also show that immunomodulation of the IL-1 pathway did not exacerbate TB disease.

Conflict of Interest Statement

The authors declare that the research was conducted in the absence of any commercial or financial relationships that could be construed as a potential conflict of interest.

Author Contributions Statement

CW, BM, CS and JF drafted and edited this manuscript. BM, JP, MS, and SN contributed to mouse experiments and/or figures. CW, PM, CC, CA, BS, HB, AW, EC, MZ, VD, PL and JF contributed to macaque experiments, data and statistically analysis and/or figures. All authors approved the final version of this manuscript.

Funding

These studies were funded by NIH UH2AI122295 (JLF and CMS). CGW was supported by NIH T32AI049820.

Acknowledgements

We thank all members of the Flynn, Sassetti, Mattila, and Lin laboratories for their collaborative efforts during this study. We are grateful for intellectual contributions from Dr. Clifton Barry III and Dr. Robert Wilkinson. Special thanks to all the veterinary and research staff for their efforts, expertise and dedication to these studies.

This manuscript has been released as a pre-print at bioRxiv (Winchell et al) (43).

Data Availability Statement:

All data are provided in a supplemental table.

References

1. WHO. Global Tuberculosis Report 2018. 2018.

2. Pasipanodya JG, Miller TL, Vecino M, Munguia G, Garmon R, Bae S, et al. Pulmonary impairment after tuberculosis. Chest. 2007;131(6):1817-24.

3. Tobin DM. Host-Directed Therapies for Tuberculosis. Cold Spring Harb Perspect Med. 2015;5(10).

4. Baindara P. Host-directed therapies to combat tuberculosis and associated non-communicable diseases. Microb Pathog. 2019;130:156-68.

5. Fremond CM, Togbe D, Doz E, Rose S, Vasseur V, Maillet I, et al. IL-1 Receptor-Mediated Signal Is an Essential Component of MyD88-Dependent Innate Response to Mycobacterium tuberculosis Infection. The Journal of Immunology. 2007;179(2):1178-89.

6. Di Paolo NC, Shafiani S, Day T, Papayannopoulou T, Russell DW, Iwakura Y, et al. Interdependence between Interleukin-1 and Tumor Necrosis Factor Regulates TNF-Dependent Control of Mycobacterium tuberculosis Infection. Immunity. 2015;43(6):1125-36.

7. Juffermans NP, Florquin S, Camoglio L, Verbon A, Kolk AH, Speelman P, et al. Interleukin-1 signaling is essential for host defense during murine pulmonary tuberculosis. J Infect Dis. 2000;182(3):902-8.

8. Mayer-Barber KD, Andrade BB, Barber DL, Hieny S, Feng CG, Caspar P, et al. Innate and adaptive interferons suppress IL-1alpha and IL-1beta production by distinct pulmonary myeloid subsets during Mycobacterium tuberculosis infection. Immunity. 2011;35(6):1023-34.

9. Mishra BB, Rathinam VA, Martens GW, Martinot AJ, Kornfeld H, Fitzgerald KA, et al. Nitric oxide controls the immunopathology of tuberculosis by inhibiting NLRP3 inflammasome-dependent processing of IL-1beta. Nat Immunol. 2013;14(1):52-60.

10. Mishra BB, Lovewell RR, Olive AJ, Zhang G, Wang W, Eugenin E, et al. Nitric oxide prevents a pathogen-permissive granulocytic inflammation during tuberculosis. Nat Microbiol. 2017;2:17072.

11. Zhang G, Zhou B, Li S, Yue J, Yang H, Wen Y, et al. Allele-specific induction of IL-1beta expression by C/EBPbeta and PU.1 contributes to increased tuberculosis susceptibility. PLoS Pathog. 2014;10(10):e1004426.

12. Maxmen A. Treatment for extreme drug-resistant tuberculosis wins US government approval. Nature 2019.

13. Tan TQ, Yogev R. Clinical pharmacology of linezolid: an oxazolidinone antimicrobial agent. Expert Rev Clin Pharmacol. 2008;1(4):479-89.

14. Coleman MT, Chen RY, Lee M, Lin PL, Dodd LE, Maiello P, et al. PET/CT imaging reveals a therapeutic response to oxazolidinones in macaques and humans with tuberculosis. Sci Transl Med. 2014;6(265):265ra167.

15. Lee M, Lee J, Carroll MW, Choi H, Min S, Song T, et al. Linezolid for treatment of chronic extensively drug-resistant tuberculosis. N Engl J Med. 2012;367(16):1508-18.

16. Iyer SS, He Q, Janczy JR, Elliott EI, Zhong Z, Olivier AK, et al. Mitochondrial cardiolipin is required for Nlrp3 inflammasome activation. Immunity. 2013;39(2):311-23.

17. Weber A, Wasiliew P, Kracht M. Interleukin-1 (IL-1) pathway. Sci Signal. 2010;3(105):cm1.

18. Furst DE. Anakinra: review of recombinant human interleukin-I receptor antagonist in the treatment of rheumatoid arthritis. Clin Ther. 2004;26(12):1960-75.

19. White AG, Maiello P, Coleman MT, Tomko JA, Frye LJ, Scanga CA, et al. Analysis of 18FDG PET/CT Imaging as a Tool for Studying Mycobacterium tuberculosis Infection and Treatment in Non-human Primates. J Vis Exp. 2017(127).

780 20. Maiello P, DiFazio RM, Cadena AM, Rodgers MA, Lin PL, Scanga CA, et al. Rhesus
781 Macaques Are More Susceptible to Progressive Tuberculosis than Cynomolgus Macaques: a
782 Quantitative Comparison. Infect Immun. 2018;86(2).
783 21. Lin PL, Maiello P, Gideon HP, Coleman MT, Cadena AM, Rodgers MA, et al. PET CT
784 Identifies Reactivation Risk in Cynomolgus Macaques with Latent M. tuberculosis. PLoS
785 Pathog. 2016;12(7):e1005739.
786 22. Cadena AM, Fortune SM, Flynn JL. Heterogeneity in tuberculosis. Nat Rev Immunol.
787 2017;17(11):691-702.
788 23. Lin PL, Pawar S, Myers A, Pegu A, Fuhrman C, Reinhart TA, et al. Early events in
789 Mycobacterium tuberculosis infection in cynomolgus macaques. Infect Immun. 2006;74(7):3790-
790 803.
791 24. Phuah JY, Mattila JT, Lin PL, Flynn JL. Activated B cells in the granulomas of nonhuman
792 primates infected with Mycobacterium tuberculosis. Am J Pathol. 2012;181(2):508-14.
793 25. Ji DX, Yamashiro LH, Chen KJ, Mukaida N, Kramnik I, Darwin KH, et al. Type I
794 interferon-driven susceptibility to Mycobacterium tuberculosis is mediated by IL-1Ra. Nat
795 Microbiol. 2019;4(12):2128-35.
796 26. Driver ER, Ryan GJ, Hoff DR, Irwin SM, Basaraba RJ, Kramnik I, et al. Evaluation of a
797 mouse model of necrotic granuloma formation using C3HeB/FeJ mice for testing of drugs
798 against Mycobacterium tuberculosis. Antimicrob Agents Chemother. 2012;56(6):3181-95.
799 27. Boettcher S, Manz MG. Regulation of Inflammation- and Infection-Driven
800 Hematopoiesis. Trends Immunol. 2017;38(5):345-57.
801 28. Lin PL, Coleman T, Carney JP, Lopresti BJ, Tomko J, Fillmore D, et al. Radiologic
802 Responses in Cynomolgus Macaques for Assessing Tuberculosis Chemotherapy Regimens.
803 Antimicrob Agents Chemother. 2013;57(9):4237-44.

804 29. Ganchua SKC, Cadena AM, Maiello P, Gideon HP, Myers AJ, Junecko BF, et al. Lymph
805 nodes are sites of prolonged bacterial persistence during Mycobacterium tuberculosis infection
806 in macaques. PLoS Pathog. 2018;14(11):e1007337.
807 30. Fung HB, Kirschenbaum HL, Ojofeitimi BO. Linezolid: an oxazolidinone antimicrobial
808 agent. Clin Ther. 2001;23(3):356-91.
809 31. Gideon HP, Phuah J, Myers AJ, Bryson BD, Rodgers MA, Coleman MT, et al. Variability
810 in tuberculosis granuloma T cell responses exists, but a balance of pro- and anti-inflammatory
811 cytokines is associated with sterilization. PLoS Pathog. 2015;11(1):e1004603.
812 32. DiFazio RM, Mattila JT, Klein EC, Cirrincione LR, Howard M, Wong EA, et al. Active
813 transforming growth factor-beta is associated with phenotypic changes in granulomas after drug
814 treatment in pulmonary tuberculosis. Fibrogenesis Tissue Repair. 2016;9:6.
815 33. Borthwick LA. The IL-1 cytokine family and its role in inflammation and fibrosis in the
816 lung. Semin Immunopathol. 2016;38(4):517-34.
817 34. Fremond CM, Togbe D, Doz E, Rose S, Vasseur V, Maillet I, et al. IL-1 receptor-
818 mediated signal is an essential component of MyD88-dependent innate response to
819 Mycobacterium tuberculosis infection. J Immunol. 2007;179(2):1178-89.
820 35. Mayer-Barber KD, Barber DL, Shenderov K, White SD, Wilson MS, Cheever A, et al.
821 Caspase-1 independent IL-1beta production is critical for host resistance to mycobacterium
822 tuberculosis and does not require TLR signaling in vivo. J Immunol. 2010;184(7):3326-30.
823 36. Cooper AM, Mayer-Barber KD, Sher A. Role of innate cytokines in mycobacterial
824 infection. Mucosal Immunol. 2011;4(3):252-60.
825 37. Scanga CA, Mohan VP, Yu K, Joseph H, Tanaka K, Chan J, et al. Depletion of CD4(+) T
826 cells causes reactivation of murine persistent tuberculosis despite continued expression of
827 interferon gamma and nitric oxide synthase 2. J Exp Med. 2000;192(3):347-58.

828 38. Ben-Sasson SZ, Hu-Li J, Quiel J, Cauchetaux S, Ratner M, Shapira I, et al. IL-1 acts
829 directly on CD4 T cells to enhance their antigen-driven expansion and differentiation. Proc Natl
830 Acad Sci U S A. 2009;106(17):7119-24.
831 39. Bajrami B, Zhu H, Kwak HJ, Mondal S, Hou Q, Geng G, et al. G-CSF maintains
832 controlled neutrophil mobilization during acute inflammation by negatively regulating CXCR2
833 signaling. J Exp Med. 2016;213(10):1999-2018.
834 40. Warsinske HC, DiFazio RM, Linderman JJ, Flynn JL, Kirschner DE. Identifying
835 mechanisms driving formation of granuloma-associated fibrosis during Mycobacterium
836 tuberculosis infection. J Theor Biol. 2017;429:1-17.
837 41. Flynn JL, Chan J, Lin PL. Macrophages and control of granulomatous inflammation in
838 tuberculosis. Mucosal Immunol. 2011;4(3):271-8.
839 42. Johnson CS, Pourbohloul SC, Furmanski P. Negative regulators of in vivo
840 erythropoiesis: interaction of IL-1 alpha and TNF-alpha and the lack of a strict requirement for T
841 or NK cells for their activity. Exp Hematol. 1991;19(2):101-5.
842 43. Caylin G. Winchell BBM, Jia Yao Phuah, Mohd Saqib, Samantha J. Nelson, Pauline
843 Maiello, Chelsea M. Causgrove, Cassaundra L. Ameel, Brianne Stein, H. Jacob Borish,
844 Alexander G. White, Edwin C. Klein, Matthew D. Zimmerman, Véronique Dartois, Philana Ling
845 Lin, Christopher M. Sassetti, JoAnne L. Flynn. Evaluation of IL-1 blockade as an adjunct to
846 linezolid therapy for tuberculosis in mice and macaques. bioRxiv: bioRxiv; 2019.

847

848 **Figure Legends**

849

850 **Figure 1. IL-1 inhibition in susceptible mice reduces inflammation with no effect on lung**
851 **bacterial burden.**

Wild type C57BL/6 and *Nos2*$^{-/-}$ mice were infected with Mtb Erdman for 2 weeks and treated with anti-IL-1R1 (αIL-1R1) for the subsequent 2 weeks. (A) Lung neutrophil (PMN) infiltration was quantified by flow cytometry; (B) Weight loss and (C) CFU in lung and (D) spleen are shown. Data shown (mean ± SD) are representative of two independent experiments. One-way ANOVA with Sidak's multiple comparisons-test was used. N=4 mice per treatment cohorts. (E) Histopathology analysis of a single lung lobe from WT or *Nos2-/-* mice was performed by Hematoxylin-eosin (H&E) staining.

Figure 2. IL-1R1 blockade combined with Linezolid ameliorates TB disease.

(A-D) C3HeB/FeJ mice were infected with Mtb Erdman for 4 weeks and treated with linezolid (LZD) and/or anti-IL-1R1 (αIL-1R1) for the following 18 days. (A) Lung neutrophils were quantified by flow cytometry; (B) Percent change in body weight is shown and (C) Bacterial burden in the lung and (D) spleen were quantified as CFU. Data shown (Mean ± SD) are representative of two independent experiments. Welch ANOVA with Dunnett's post-test was used to calculate statistical significance where each treatment group was compared to the vehicle as control group. N=3-5 mice per treatment group. (E-G) C3HeB/FeJ mice were infected with *M. tb* Erdman for 8 weeks and treated with linezolid (LZD) and/or an inhibitor of the NLRP3 inflammasome (MCC950) for the following 21 days. (E) Lung neutrophils were quantified by flow cytometry. (F) Bacterial burden in the lung was quantified by CFU. Data shown (Mean ± SD) are from one experiment. One-way ANOVA with Tukey's multiple comparison test was used to calculate the p-value. N=4-5 mice/group. (G) Representative immunofluorescence images of the lungs from different treatment groups. Cell nuclei stained with DAPI (blue), T-cells stained with anti-mouse CD3ε (green) and neutrophils stained with anti-mouse Ly-6G (red).

Figure 3. Erythropoiesis associated with LZD treatment was partially relieved after IL-1R1 blockade.

C3HeB/FeJ mice were infected with Mtb Erdman for 4 weeks, and treated with LZD either alone or in combination with anti-IL-1R1 antibody for the subsequent 18 days. (A) Gating strategy for detecting erythroid progenitors is shown. Erythroid progenitors in the spleen (B-C) and bone marrow (D-E) were quantified by flow cytometry as described in Materials and Methods. Representative flow cytometry plots and percent changes in the early erythroid progenitors (Pro-Ery, EryA, EryB) among different treatment groups are shown. Data shown (Mean ± SD) are from two independent experiments. One-way ANOVA with Dunnett's post-test was applied to calculate the p-value by comparing the mean of each group with that of LZD treated group. N=3-5 mice per group.

Figure 4. HDT reduces granuloma inflammation by PET/CT in macaques

Cynomolgus macaques were infected with *Mtb* Erdman for approximately 4 months (see Supplementary Table 1) and randomized to treatment with LZD or LZD+IL-1Rn for an additional 4 weeks. PET CT scans were performed pre-treatment 0, 2 and 4 weeks post-treatment with 4 week scans as the last prior to necropsy. (A) 3-D renderings of PET/CT scans from pre-treatment and 4 weeks post-treatment are depicted, with "best" and "worst" of each group referring to TB disease prior to drug administration. (B) Total lung FDG activity of each macaque throughout treatment with LZD (left) or LZD+IL-1Rn (right). Two-way ANOVA with Dunnett's adjusted p-values are reported. (C) Individual granulomas were identified pre-treatment and tracked post-treatment by PET/CT. Change in size (by CT) was determined for granulomas from each animal; the median (left) change in granuloma size from each animal and individual granulomas per animal (right). (D) Standard uptake value (SUVR) of ^{18}F-FDG was calculated for each granuloma, representing inflammation. The median change in SUVR of all granulomas (left) and change in SUVR of individual granulomas from each animal (right) are shown. Mann-Whitney tests determined p values for (C) and (D), with $p<0.05$ considered significant.

Figure 5. Addition of IL-1Rn does not modify efficacy of LZD-bacterial killing

Bacterial burden is shown after 4 weeks of LZD (blue) or LZD+IL-1Rn (red) treatment. (A) Total thoracic (lung + lymph nodes) and lung CFU; each data point represents one macaque. Total thoracic CFU from 3 similarly infected untreated historical control macaques (black) are included as reference for untreated CFU at this time point, but excluded from statistical analysis. (B) The percent of all lung granulomas that were CFU+ per monkey. (C) CFU of all thoracic lymph nodes with data points representing CFU from one macaque. CFU+ lymph nodes show the CFU from each thoracic lymph node in any animal that was Mtb+. For (A) and (B), p values were determined by Mann-Whitney test. (C) PET/CT scans from pre-treatment were used to model predicted CFU prior to HDT initiation and compared to actual CFU determined at time of necropsy. The predicted change in CFU was determined by: Actual total thoracic CFU post-treatment– Predicted total thoracic CFU interval (predicted from pre-drug-treatment scan). Bars represent mean of prediction intervals and error whiskers represent the lower and upper bounds of the difference between final total CFU and predicted CFU prior to drug treatment.

Figure 6. Linezolid-associated bone marrow suppression was not observed in macaques

Bone marrow was acquired from the sternum of all macaques at necropsy after 4 weeks LZD or LZD+IL-1Rn. A portion was used for flow cytometric analysis of erythroid progenitor populations and the rest for histopathology analysis. (A) A schematic of erythropoiesis indicating the stage of differentiation and corresponding expression levels of phenotyping markers (CD235a and CD71) and progenitor ratios (1:2:4:8). Included is the gating strategy to identify progenitor populations and an example of MitoTracker staining. (B) The ProE:EryC ratio (left) of each animal, including untreated TB only macaques (black) from other ongoing unpublished studies. A single uninfected animal (open circle) is shown as reference, the dotted line indicates the homeostatic ratio of 1:8. MitoTracker MFI (right) is shown for each macaque per treatment

group. Kruskal-Wallis test was performed to compare the three groups (excluding uninfected macaque) and p values are shown in the graphs. (C) Representative H&E images from sternal bone marrow acquired at necropsy, 20x (left) and 40x (right) are shown.

Figure 7. HDT reduces inflammatory signatures in BAL

Bronchoalveolar lavages (BAL) were acquired pre-treatment and 3 weeks post-treatment with LZD (blue) or LZD+IL-1Rn (red). (A) Cells were analyzed by flow cytometry to determine frequency changes in CD4 T cells (CD3+CD4+), CD8 T cells (CD3+CD8+), macrophages (CD11b+CD206+) and neutrophils (CD11b+Calprotectin+). Wilcoxon signed rank test was performed to determine differences before and after drug treatment, regardless of group (LZD and LZD+IL-1Rn combined). (B) BAL fluid was concentrated 10X and assessed by multiplex assay for changes in inflammatory cytokines and chemokines for a random subset of samples (n=3 per treatment group). Wilcoxon signed rank test was performed to determine differences before and after drug treatment, regardless of group (LZD and LZD+IL-1Rn combined).

Figure 8. Inflammation modulation by HDT influences granuloma resolution

(A) Randomly selected granulomas (n=5 per macaque, n=25 per treatment group) were subjected to multiplex cytokine analysis to determine differences between treatment groups (colors indicate lesions from a single animal). p values shown determined by Mann-Whitney test. (B) A linear regression analysis of IL-1β levels and fold change in SUVR is depicted for LZD (blue) and LZD+IL-1Rn (red) granulomas. R^2 and p values are provided in the legend. (C) Granulomas from LZD (n=57) and LZD+IL-1Rn (n=45) were examined by a pathologist (EK) and categorized. We compared fibrotic (red) vs non-fibrotic (gray) (left) frequencies between treatment groups. The right compares necrotizing (red) vs non-necrotizing (blue) and other (gray) granuloma frequencies. Fisher's exact test p-values are reported.

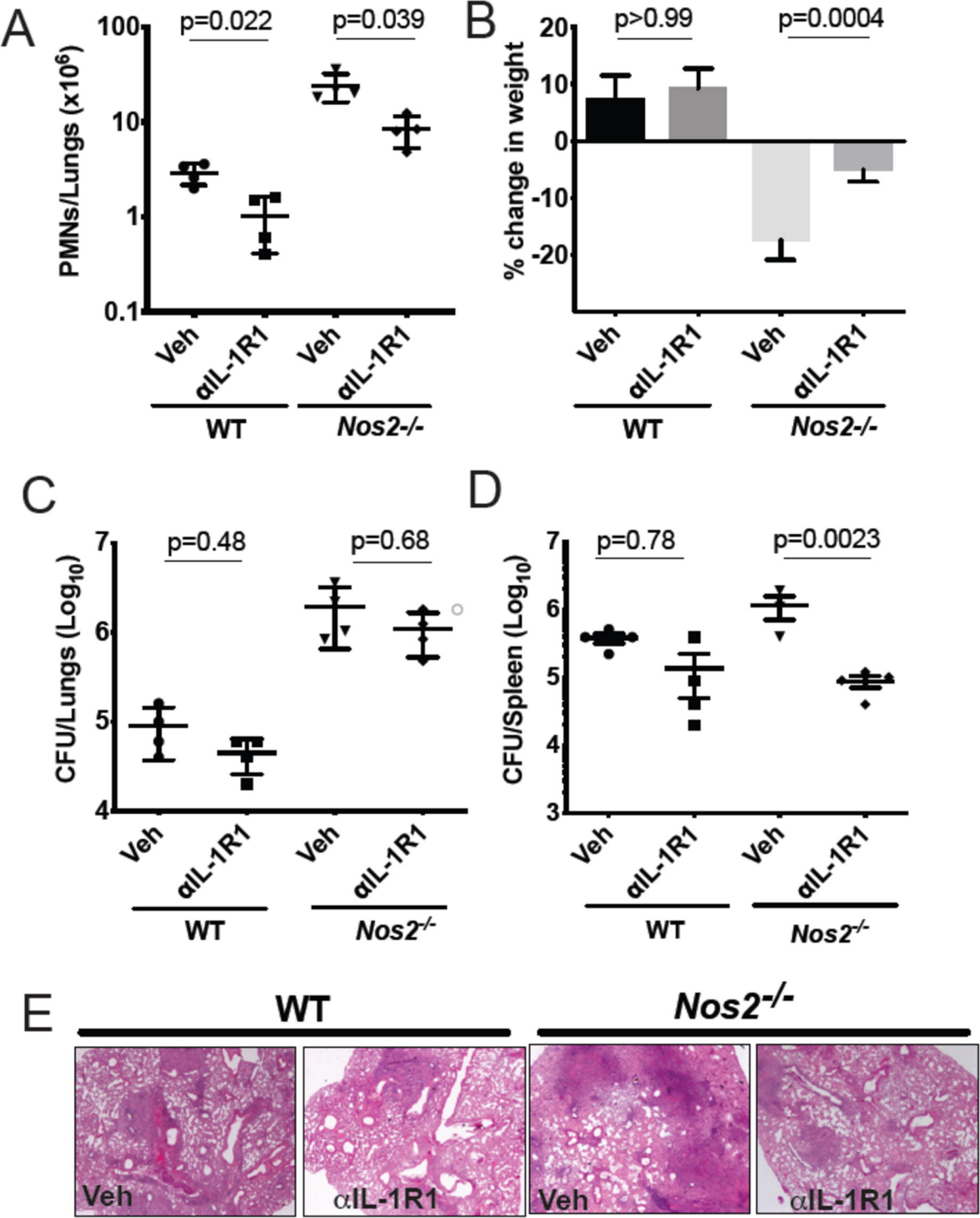
A
PMNs/Lungs (x10^6)
100
10
1
0.1
p=0.022
p=0.039
Veh
αIL-1R1
Veh
αIL-1R1
WT
Nos2-/-
B
% change in weight
20
10
0
-10
-20
p>0.99
p=0.0004
Veh
αIL-1R1
Veh
αIL-1R1
WT
Nos2-/-
C
CFU/Lungs (Log10)
7
6
5
4
p=0.48
p=0.68
Veh
αIL-1R1
Veh
αIL-1R1
WT
Nos2-/-
D
CFU/Spleen (Log10)
7
6
5
4
3
p=0.78
p=0.0023
Veh
αIL-1R1
Veh
αIL-1R1
WT
Nos2-/-
E
WT
Nos2-/-
Veh
αIL-1R1
Veh
αIL-1R1

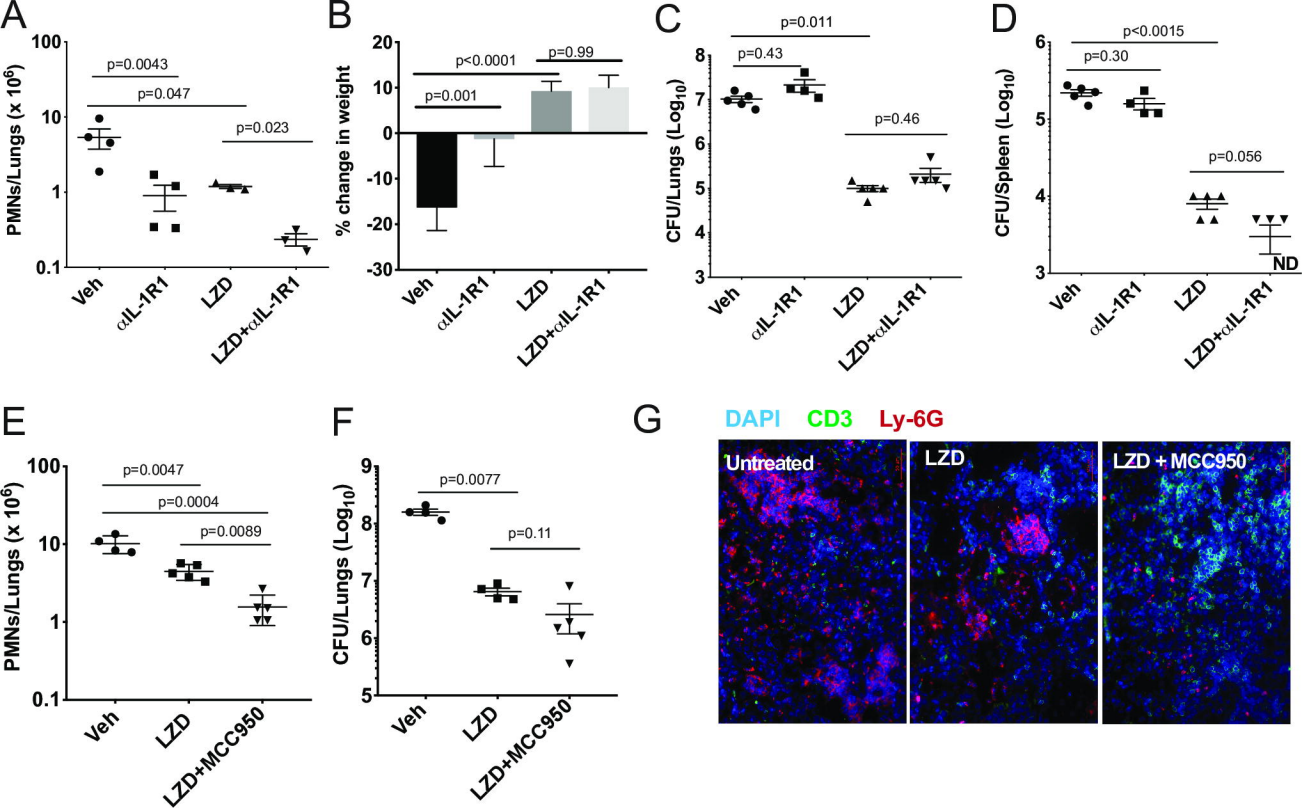
A
PMNs/Lungs (x 10^6)
p=0.0043
p=0.047
p=0.023
Veh
αIL-1R1
LZD
LZD+αIL-1R1
B
% change in weight
p<0.0001
p=0.99
p=0.001
C
CFU/Lungs (Log10)
p=0.011
p=0.43
p=0.46
D
CFU/Spleen (Log10)
p<0.0015
p=0.30
p=0.056
ND
E
PMNs/Lungs (x 10^6)
p=0.0047
p=0.0004
p=0.0089
LZD+MCC950
F
CFU/Lungs (Log10)
p=0.0077
p=0.11
G
DAPI
CD3
Ly-6G
Untreated
LZD
LZD + MCC950

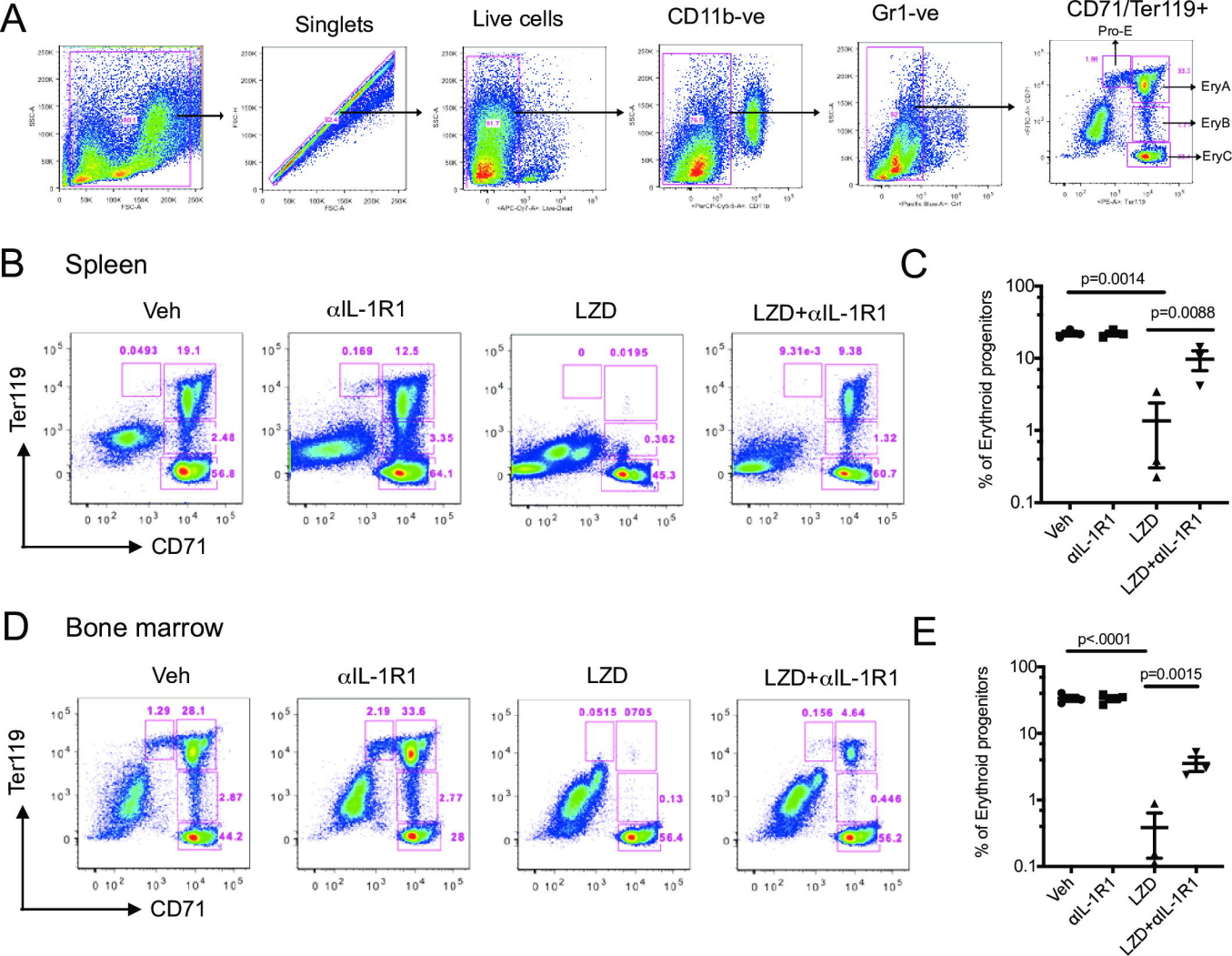
A
Singlets
Live cells
CD11b-ve
Gr1-ve
CD71/Ter119+
Pro-E
EryA
EryB
EryC
B
Spleen
Veh
αIL-1R1
LZD
LZD+αIL-1R1
Ter119
CD71
0.0493
19.1
2.48
56.8
0.169
12.5
3.35
64.1
0
0.0195
0.362
45.3
9.31e-3
9.38
1.32
60.7
C
% of Erythroid progenitors
p=0.0014
p=0.0088
Veh
αIL-1R1
LZD
LZD+αIL-1R1
D
Bone marrow
Veh
αIL-1R1
LZD
LZD+αIL-1R1
Ter119
CD71
1.29
28.1
2.87
44.2
2.19
33.6
2.77
28
0.0515
0705
0.13
56.4
0.156
4.64
0.446
56.2
E
% of Erythroid progenitors
p<.0001
p=0.0015
Veh
αIL-1R1
LZD
LZD+αIL-1R1

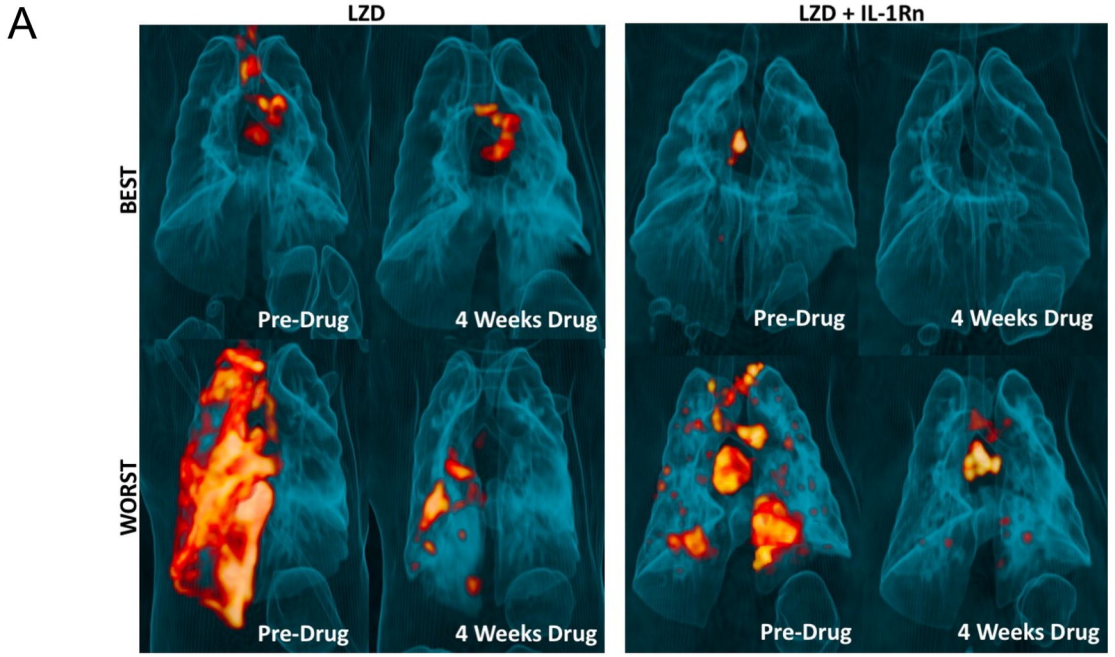
A
LZD
LZD + IL-1Rn
BEST
WORST
Pre-Drug
4 Weeks Drug
Pre-Drug
4 Weeks Drug
Pre-Drug
4 Weeks Drug
Pre-Drug
4 Weeks Drug

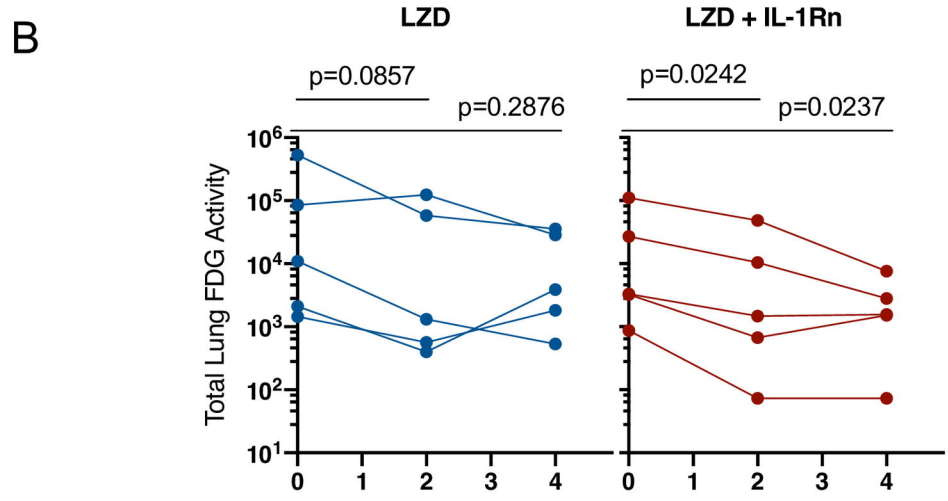
B
LZD
LZD + IL-1Rn
p=0.0857
p=0.2876
p=0.0242
p=0.0237
Total Lung FDG Activity
10^6
10^5
10^4
10^3
10^2
10^1
0
1
2
3
4
0
1
2
3
4

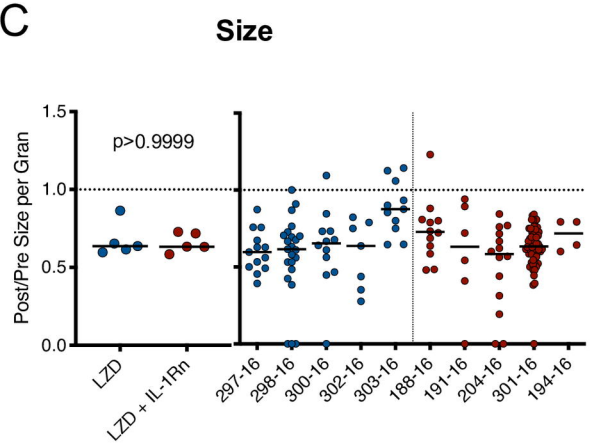
C
Size
p>0.9999
Post/Pre Size per Gran
1.5
1.0
0.5
0.0
LZD
LZD + IL-1Rn
297-16
298-16
300-16
302-16
303-16
188-16
191-16
204-16
301-16
194-16

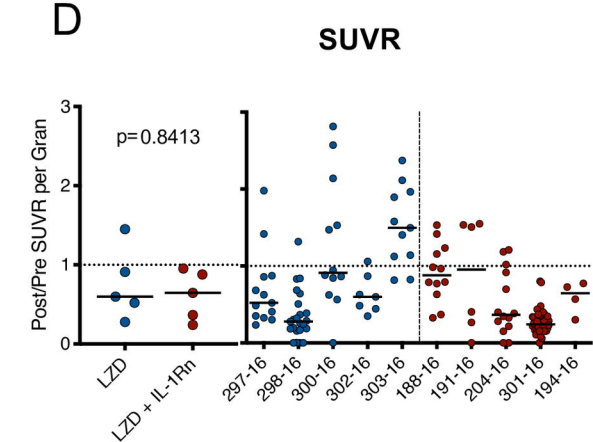
D
SUVR
p=0.8413
Post/Pre SUVR per Gran
3
2
1
0
LZD
LZD + IL-1Rn
297-16
298-16
300-16
302-16
303-16
188-16
191-16
204-16
301-16
194-16

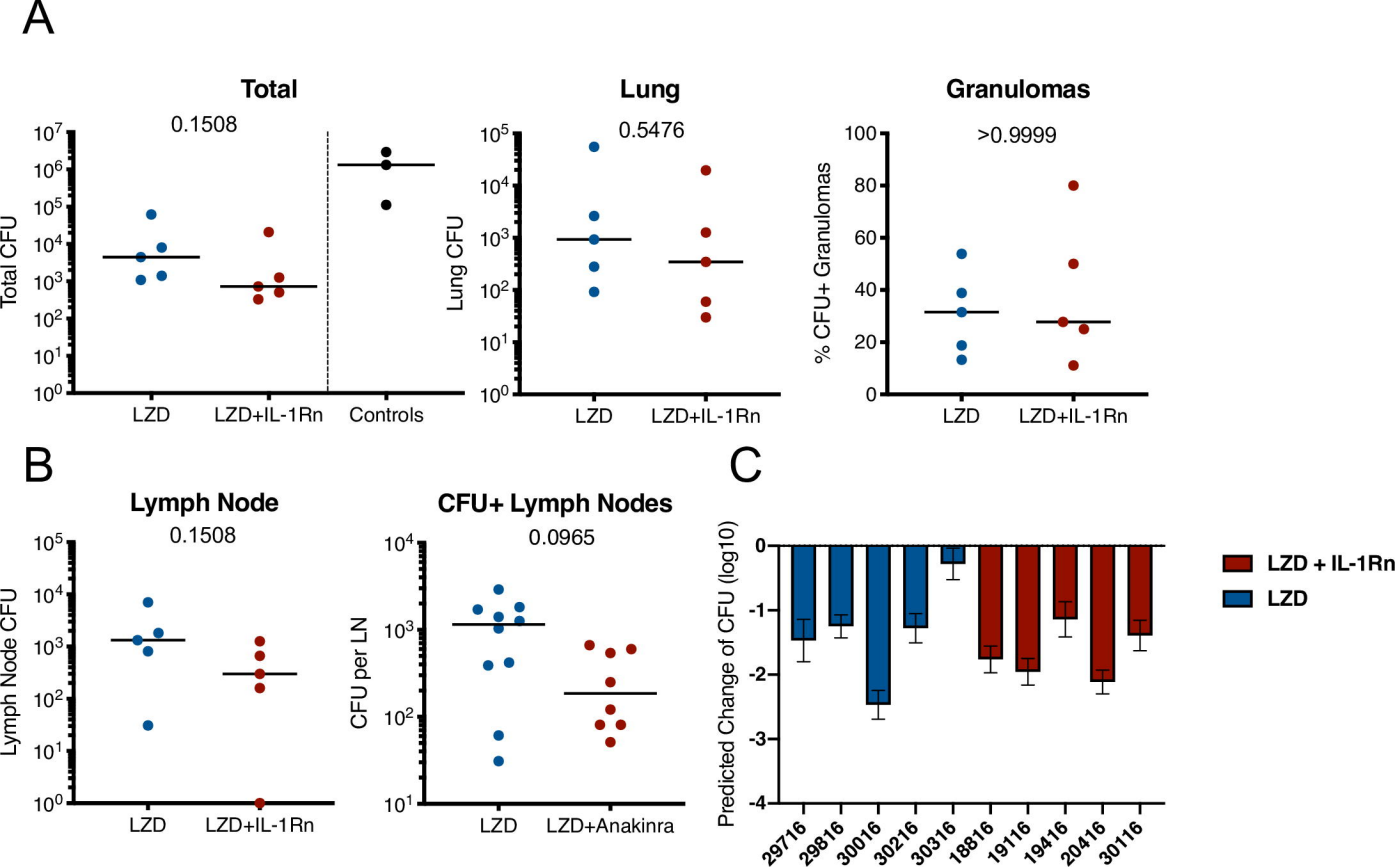
A
Total
0.1508
Total CFU
LZD
LZD+IL-1Rn
Controls
Lung
0.5476
Lung CFU
LZD
LZD+IL-1Rn
Granulomas
>0.9999
% CFU+ Granulomas
LZD
LZD+IL-1Rn
B
Lymph Node
0.1508
Lymph Node CFU
LZD
LZD+IL-1Rn
CFU+ Lymph Nodes
0.0965
CFU per LN
LZD
LZD+Anakinra
C
Predicted Change of CFU (log10)
LZD + IL-1Rn
LZD
29716
29816
30016
30216
30316
18816
19116
19416
20416
30116

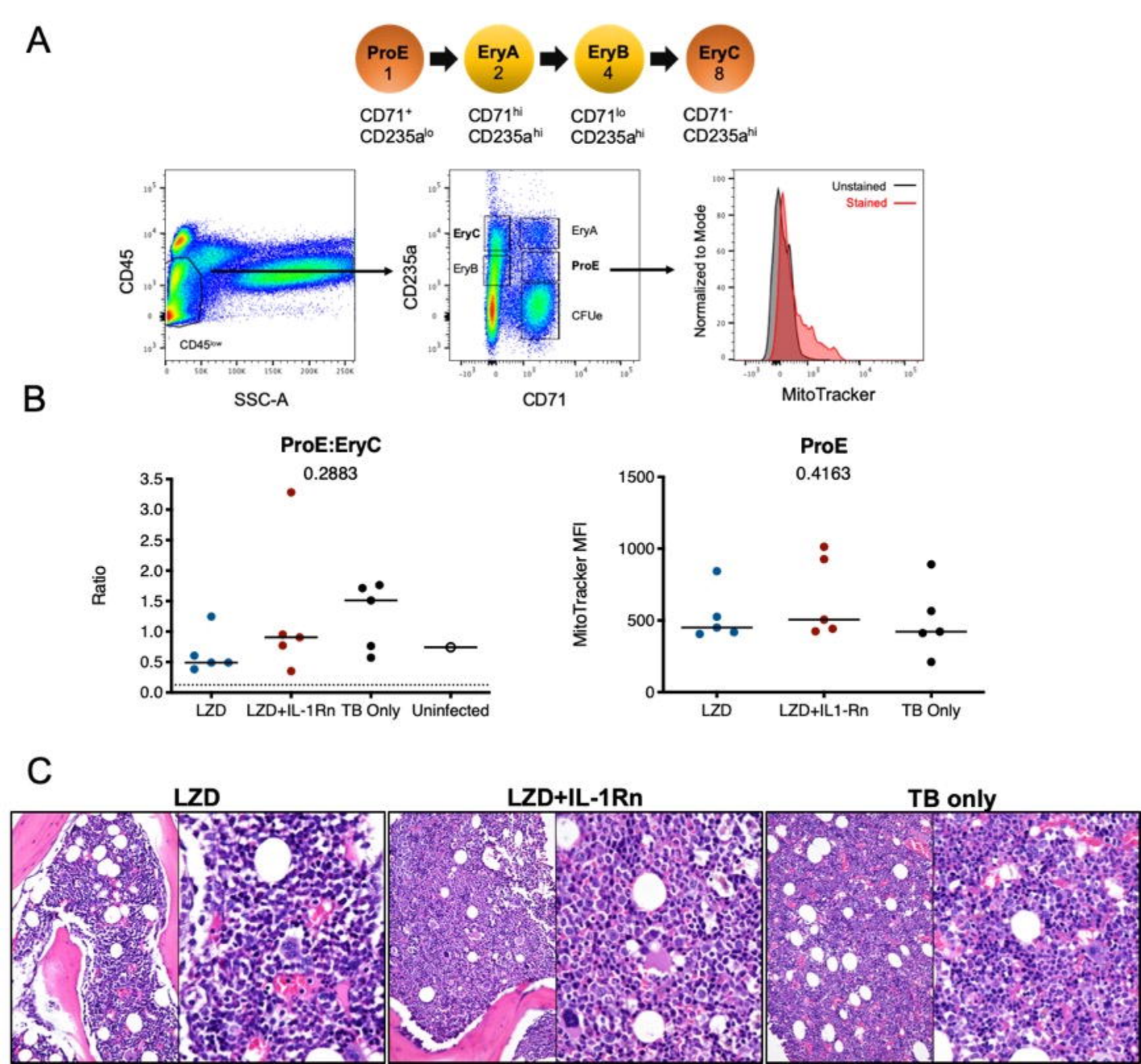
A
ProE
1
EryA
2
EryB
4
EryC
8
CD71+ CD235alo
CD71hi CD235ahi
CD71lo CD235ahi
CD71- CD235ahi
CD45
SSC-A
CD45low
CD235a
CD71
EryC
EryB
EryA
ProE
CFUe
Normalized to Mode
MitoTracker
Unstained
Stained
B
ProE:EryC
0.2883
Ratio
LZD
LZD+IL-1Rn
TB Only
Uninfected
ProE
0.4163
MitoTracker MFI
LZD
LZD+IL1-Rn
TB Only
C
LZD
LZD+IL-1Rn
TB only

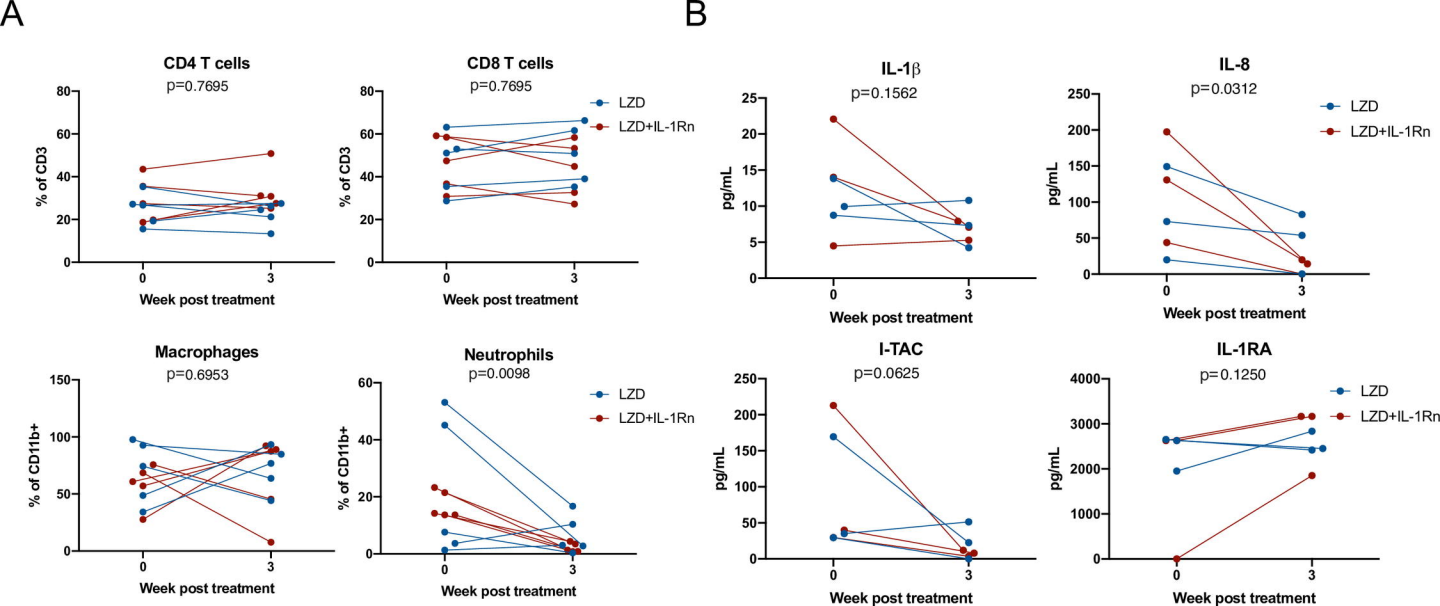
A
CD4 T cells
p=0.7695
% of CD3
Week post treatment
CD8 T cells
p=0.7695
LZD
LZD+IL-1Rn
Macrophages
p=0.6953
% of CD11b+
Neutrophils
p=0.0098
B
IL-1β
p=0.1562
pg/mL
IL-8
p=0.0312
I-TAC
p=0.0625
IL-1RA
p=0.1250

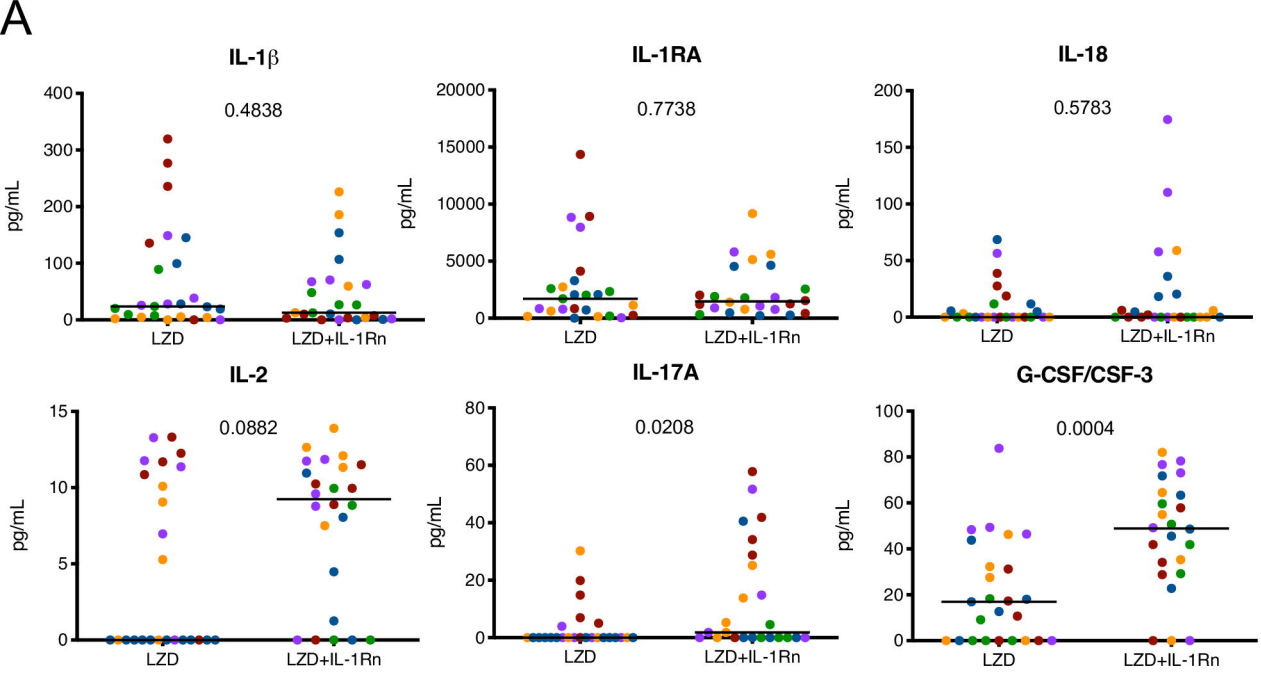
A
IL-1β
0.4838
IL-1RA
0.7738
IL-18
0.5783
IL-2
0.0882
IL-17A
0.0208
G-CSF/CSF-3
0.0004
pg/mL
LZD
LZD+IL-1Rn

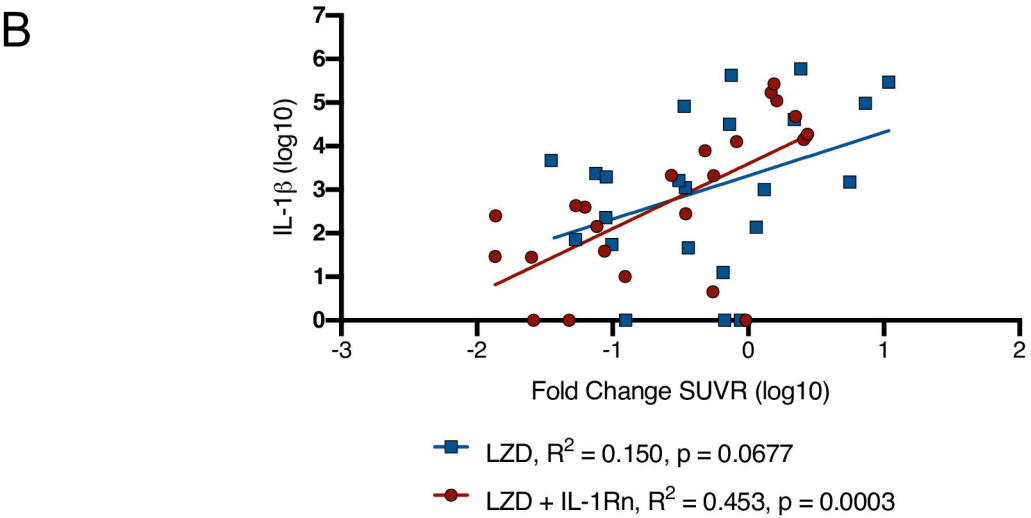
B
IL-1β (log10)
Fold Change SUVR (log10)
LZD, R2 = 0.150, p = 0.0677
LZD + IL-1Rn, R2 = 0.453, p = 0.0003

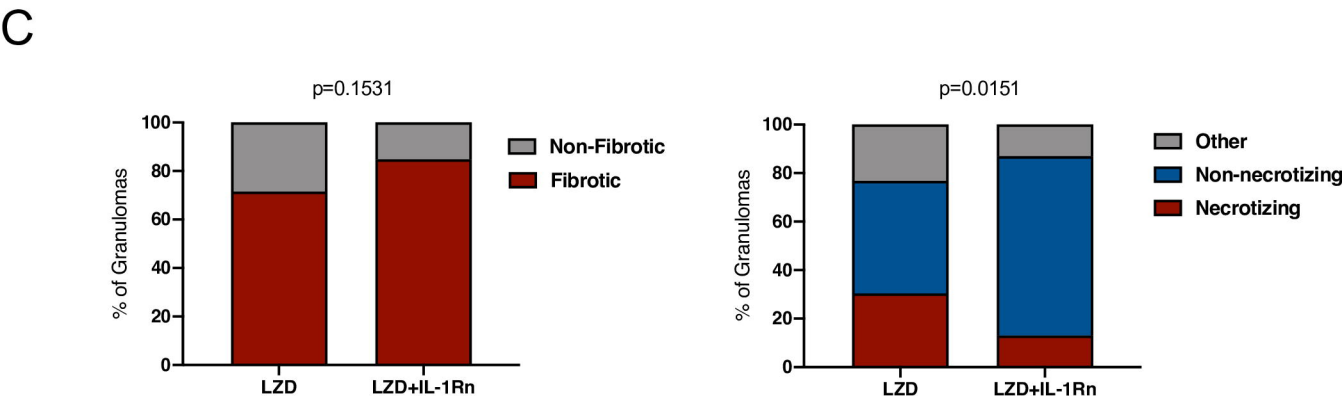
C
p=0.1531
% of Granulomas
Non-Fibrotic
Fibrotic
LZD
LZD+IL-1Rn
p=0.0151
Other
Non-necrotizing
Necrotizing